RIGA TECHNICAL UNIVERSITY

Anna Bystrova

STRUCTURAL IMPERFECTIONS OF THE HYDROXYAPATITE SURFACE LAYER TO ENGINEER ITS ELECTRICAL POTENTIAL

Summary of the Doctoral Thesis

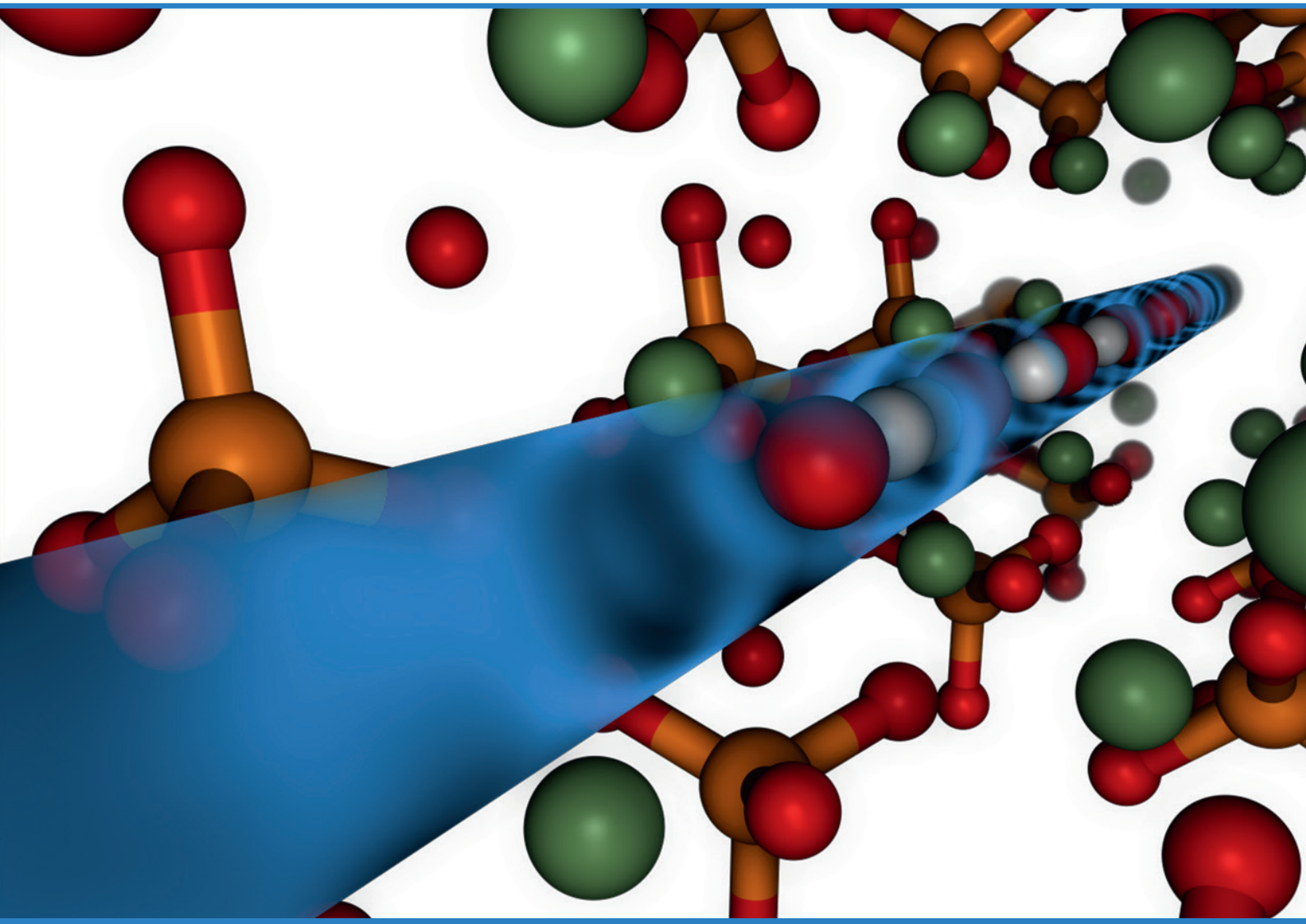

RTU Press
Riga 2021

RIGA TECHNICAL UNIVERSITY
Faculty of Materials Science and Applied Chemistry

Anna Bystrova
Doctoral Student of the Study Programme "Materials Science"

STRUCTURAL IMPERFECTIONS OF THE HYDROXYAPATITE SURFACE LAYER TO ENGINEER ITS ELECTRICAL POTENTIAL

Summary of the Doctoral Thesis

Scientific supervisor
Professor Dr. habil. phys.
JURIJS DEHTJARS

RTU Press
Riga 2021

Bystrova, A. Structural Imperfections of the Hydroxyapatite Surface Layer to Engineer Its Electrical Potential. Summary of the Doctoral Thesis. Riga: RTU Press, 2021. 54 p.

Published in accordance with the decision of the Promotion Council "RTU P-02" of 9 March 2021, Minutes No. 04030-9.2.1/2.

Acknowledgements

I would like to express my deepest appreciation to my supervisor Professor Dehtjars for his patience and great ideas without which the writing of this Thesis would not have been possible and for the opportunity to work in his team.

I would like to express my deepest appreciation to Ekaterina Paramonova, Jose Coutinho and Vladimir Bystrov for their help in the work in computer simulation and theoretical modelling.

I would like to thank my colleague Professor Katashev and ex-colleague Alexander Sudnikovich for their invaluable help in the 'battle' with the experimental setup as well as for discussions of experimental results.

I would like to thank PERCERAMIC project employees for supplying the samples, my ex-colleague Linda Lancere for taking the investigated samples for gamma-ray radiation at the Riga East University Hospital, a colleague from the Faculty of Materials Science and Applied Chemistry who did hydrogenation, and Professor Popov's team who measured HAp samples at DESY.

I would like to thank RTU for financial support of my research.

My special thanks go to the team of Institute of Mathematical Problems of Biology, especially to Professor Vladimir Bystrov, for their support during all this work as well as to the Russian Foundation for Basic Research (RFBR) for partial support through grant #19-01-00519_A.

Special thanks go to Martins Misans for his suggestions regarding the context and Sanja for her general emotional support during all this time.

https://doi.org/10.7250/9789934226403
ISBN 978-9934-22-640-3 (pdf)

DOCTORAL THESIS PROPOSED TO RIGA TECHNICAL UNIVERSITY FOR THE PROMOTION TO THE SCIENTIFIC DEGREE OF DOCTOR OF SCIENCE

To be granted the scientific degree of Doctor of Science (Ph. D.), the present Doctoral Thesis has been submitted for the defence at the open meeting of RTU Promotion Council on 28 June 2021 at 15.00 at the Faculty of Materials Science and Applied Chemistry of Riga Technical University, 3/7 Paula Valdena Street, Room 272.

OFFICIAL REVIEWERS

Professor Dr. habil. phys. Andris Ozols
Riga Technical University, Latvia

Professor Dr. habil. phys. Donāts Millers
Institute of Solid State Physics, University of Latvia, Latvia

Ph. D. Maria Sedelnikova,
National Research Tomsk State University, Russia

DECLARATION OF ACADEMIC INTEGRITY

I hereby declare that the Doctoral Thesis submitted for the review to Riga Technical University for the promotion to the scientific degree of Doctor of Science (Ph. D.) is my own. I confirm that this Doctoral Thesis had not been submitted to any other university for the promotion to a scientific degree.

Anna Bystrova ……. (signature)

Date: ……

The Doctoral Thesis has been written in English. It consists of an Introduction; 3 Chapters; Conclusion; 133 figures; 14 tables; 2 appendices; the total number of pages is 163, including appendices. The Bibliography contains 119 titles.

CONTENTS

ABBREVIATIONS

HAp – hydroxyapatite
PE – photoelectron
NP – nanoparticle
DFT – density functional theory
BIO+ (CHARMM) – implementation of the Chemistry at HARvard Macromolecular Mechanics force field
OPLS – Optimized Potentials for Liquid Simulations
PM3 – Austin model 1 reparametrization
AIMPRO – ab initio modelling program
DOS – density of states
PL – photoluminescence
MM – molecular mechanics
QM – quantum mechanics
RHF – restricted Hartree–Fock approximation
UHF – unrestricted Hartree–Fock approximation
EWF – electron work function
LDA – linear density approximation
DESY – Deutsches Elektronen Synchrotron
EBSD – electronic band structure diagram
MW – microwave

GENERAL OVERVIEW OF THE THESIS

Thesis topic rationale

Hydroxyapatite (HAp) is the most widely used material for the production of bone implants. The number of patients that need operations to restore the integrity of the bone is growing (in comparison with rates in 1990, by 2050 the worldwide incidence of hip fracture in men is projected to increase by 310 % and in women by 240 % [23]). The main risk of using bone implants is its possible incompatibility with the host bone. To decrease this risk, the implant material should have high biocompatibility properties. For this, the bone cells that regenerate the bone tissue and are compatible with an implant have to be adhered on the implant's surface [2, 42]. To adhere living cells, it is necessary to adjust the electrical potential on HAp surface [7–21]. The research on formation of HAp surface electrical charges (or polarization) and the engineering of surface electrical potential is in its beginning stage.

HAp contains structural defects and has non-stoichiometric composition. Defects induce the heterogeneity of the surface electrical potential. However, the role and influence of various HAp's surface structural defects in the formation of HAp energy band structure and HAp electron work function value has not yet been investigated enough. The combination of experimental and computational methods provides an opportunity to establish and estimate the role and effect of each individual type of defect on the electrical charge of the HAp surface. This will help to improve the technology of producing HAp implants.

The present research is devoted to exploration of the features of HAp structure that are able to control the electrical potential of its surface.

Aim and tasks of the Thesis

The goal of this research is to identify the influence of HAp defects (such as OH group, H, O atom vacancies, H atom interstitials, and their combination) on the electrical potential of HAp's surface.

To achieve the aim of the Thesis, the following tasks have been put forward:

1) to construct theoretical models for determining the electrical properties of HAp structures with defects;
2) to carry out theoretical research to determine the electrical properties of HAp structures with defects by evaluating the electrical polarization of HAp clusters containing defects;
3) generating different types of defects in order to carry out an experimental study on determining the electrical properties of HAp structures with defects. To induce defects by using annealing, hydrogenation, MW and gamma-ray irradiation. Such point defects as O-vacancies should be produced under the influence of applied gamma radiation. The hydrogenation should evaluate the intrusion of protons into the interior and changes of the surface charge. MW radiation promotes the motion of protons along OH-channel. Using synchrotron-induced photoluminescence (PL), to identify

local levels of HAp structures with defects in the forbidden band and investigate the deep levels of HAp;

4) to carry out the experiments on determining the electrical potential of HAp surface depending on the presence of defects using EWF measurements;
5) to compare the theoretical and experimental research results and to give suggestions on implementation of the producing technology of HAp modified structures with different types of structural imperfections.

Scientific novelty

The following scientific results have been obtained for the first time.

1. Theoretical and experimental approaches were used together to investigate the influence of structural imperfections (OH-, H-, O-vacancies, H-interstitials, and hydrogen atoms filling unsaturated hydrogen bonds) on HAp electrical properties. The computer simulations of HAp structures with various defects (vacancies, interstitials) were made to analyse their properties. Analysis of structural imperfections (OH-, H-, O-vacancies, H-interstitials, and hydrogen atoms filling unsaturated hydrogen bonds) influence on HAp surface electrical potential was done. Also, studies of HAp surface by methods of photoluminescence (PL) emission and synchrotron excitation spectroscopy, and threshold photoelectron (PE) emission spectroscopy were performed.
2. Annealing, hydrogenation, MW and gamma-ray irradiation and their combination influence on HAp structure were investigated experimentally. The results were compared with computational data.
3. Analyses of HAp sample PL excitation spectra at energy level of 2.95 eV was done. This level is the recombination centre. Using PL levels corresponding to the deep levels (named as A, B, C, D levels) were established experimentally. These levels were previously known only in theoretical calculations.
4. The roles of OH-, H-, O- vacancies, H-interstitials, and hydrogen atoms filling unsaturated hydrogen bonds in the HAp electrical charge changes were established.

Theses to defend

1. Structural defects of HAp that affect the electrical potential of the HAp surface:
   a) OH-vacancies:
      - induce additional energy levels inside forbidden band $E_i \approx E_c$ – (2.4–1.7) eV or $E_i \approx E_v$ + (3.1–3.8) eV (hereafter E_i – additional energy levels in the forbidden band, E_v – top of the valence band, E_c – bottom of the conductive band). These levels can serve as electron donors and acceptors or recombination (electron-hole) centres;
      - increase the value of the forbidden band (E_g) by ~0.9 eV ($E_g \approx 4.6$ eV in the case of HAp structure without defects).
   b) The hydrogen filling in the unsaturated hydrogen bonds:

- induces two additional energy levels $E_{i1} \approx E_c - 2.92$ eV and $E_{i2} \approx E_c - 3.74$ eV; this level is completely occupied by electrons;
- increases E_g by ~0.03 eV.

c) H-interstitials:
- induce energy levels inside HAp forbidden band $E_i \approx E_c - (3.1–3.9)$ eV. These levels serve as recombination centres of electrons;
- increase E_g by ~0.5 eV.

d) H- and O-vacancies:
- induce additional energy levels inside the HAp forbidden band, close to the top of valence band ($E_i \approx E_v + 0.1$ eV), and increase the width of forbidden band by ~0.3–0.5 eV.

2. The gamma radiation, annealing, hydrogenation, MW irradiation can be used to regulate the HAp surface electrical potential by changing HAp structural imperfections.
The induced defects (OH-, H-, O-vacancies, H-interstitials, and hydrogen atoms filling unsaturated hydrogen bonds) remain on the HAp surface for at least 11 months.
The induced defects allow regulating the electrical potential of the HAp surface, which was estimated by electron work function, changing from 4.6 eV ± 0.1 eV to 5.49 eV ± 0.10 eV.

The following modes are recommended for producing structural imperfections:
- for induction of OH-vacancies: annealing at 542–546 °C for 30 minutes; 10 Gy dose of ionizing radiation, distance from the radiation source to the sample – 1 metre, radiation area – 10 cm × 10 cm, hydrogenation at t = 23 °C and (60 ± 2) atm for 6 hours;
- for hydrogen filling in the unsaturated hydrogen bonds: annealing at 542–546 °C for 30 minutes;
- for inducing of H-interstitials: MW radiation for 6.5 minutes at 800 W; hydrogenation at t = 23 °C and (60 ± 2) atm for 6 hours;
- for induction of H-vacancies: annealing at 542–546 °C for 30 minutes; 10 Gy dose of ionizing radiation, distance from the radiation source to the sample – 1 m, radiation area – 10 cm × 10 cm, hydrogenation at t = 23 °C and (60 ± 2) atm for 6 hours;
- for induction of O-vacancies: annealing at 542–546 °C for 30 minutes; MW radiation in 6.5 minutes with 800 W power; hydrogenation at t = 23 °C and (60 ± 2) atm for 6 hours.

Research methods

In this Thesis, theoretical and experimental approaches were used together to investigate the influence of structural imperfections on HAp electrical properties.

Molecular mechanics (MM) methods (with force fields such as BIO+ (CHARMM) (application of force field “Chemistry in HARvard’s macromolecular mechanics”) and OPLS (potentials optimized for liquid simulations), quantum semi-empirical method PM3 (Austin

model 1 reparameterization) as well as DFT (density functional theory) (AIMPRO code (ab initio modeling program)) were used for theoretical calculations. They were used to construct models of crystalline HAp structures with and without structural defects (H-interstitial, OH-, O-, H-vacancy, hydrogen filling of unsaturated hydrogen bonds). Calculations were performed on the scale of both HAp unit cell and cluster (different sizes and shapes).

The studies on HAp surface charge were made by methods of photoluminescence (PL) emission and synchrotron excitation spectroscopy, and threshold photoelectron (PE) emission spectroscopy.

Practical significance

The results of the Thesis have practical importance for medicine and nanotechnology. The understanding of the formation mechanisms of different structural imperfections gives an opportunity to influence these processes and, therefore, to modify HAp bioimplant surface as needed for practical applications.

The new knowledge about treatment influence on HAp surface obtained as results of this Thesis offers a new practical background for further design of bioimplants using recommendations developed in the work about the types and properties of HAp structural imperfections.

Approbation of the Thesis

The results of work were reported at the following scientific conferences

1. International Conference “MATERIAS-2017”, April 9–12, 2017, Aveiro, Portugal;
2. XXI All-Russian Conference on the Physics of Ferroelectrics (VCS-XXI) (In Russian), June 26–30, 2017, Kazan, Russia; (This poster report received the prize of the Conference of the VCS-XXI as the best poster presentation among young scientists);
3. Second International Workshop Modern Nanotechnologies (IWMN-2). August 27–29, 2016, Ekaterinburg, Russia;
4. VI International Conference “Mathematical biology and bioinformatics”, October 16–21, 2016, Pushchino, Russia;
5. 20th International Pushchino School-Conference of Young Scientists “Biology is the science of the 21st century”, April 18–22, 2016, Pushchino, Russia;
6. International Workshop “Modern Nanotechnologies”, August 25–27, 2015, Ekaterinburg, Russia;
7. Conference of young scientists “Biology is the science of 21 century”, April 20–24, 2015, Pushchino, Russia;
8. 5th International Conference on Mathematical Biology and Bioinformatics, October 19–24, 2014, Pushchino, Russia;
9. The Second Baltic Neutron School, May 5–8, 2014, Tartu, Estonia;
10. International Conference “Piezoforce Microscopy and Nanoscale Phenomena in Polar Materials”, July 14–17, 2014, Ekaterinburg, Russia;

11. International Symposium on Applications of Ferroelectric and Workshop on Piezoresponse Force Microscopy (ISAF/PFM), July 21–25, 2013, Prague, Czech Republic;
12. 9th International Conference on Bionics and Prosthetics, Biomechanics and Mechanics, Mechatronics and Robotics (ICBBM 2013), June 17–21, 2013, Riga, Latvia;
13. International conference "Functional Materials and Nanotechnology" (FM & NT-2012), April 17 – 20, 2012, Riga, Latvia;
14. The 21st IEEE International Symposium on Applications of Ferroelectrics (ISAF), the 11th European Conference on the Applications of Polar Dielectrics (ECAPD), and the 4th Conference on Piezoresponse Force Microscopy and Nanoscale Phenomena in Polar Materials (PFM) (ISAF-ECAPD-PFM-2012), July 9–13, 2012, Aveiro, Portugal;
15. International Symposium on Biomedical Engineering and Medical Physics, in cooperation with IFMBE under the umbrella of the Riga Technical University 53rd International Scientific Conference Dedicated to the 150th Anniversary of the Riga Technical University and The 1st Congress of World Engineers and Riga Polytechnical Institute / RTU Alumni, October 11–12, 2012, Riga, Latvia;
16. 1st International School on Surface Science "Technologies and Measurements on Atomic Scale" (SSS-TMAS), 28 Sept. – 2 October, 2011, Veliky Novgorod, Russia;
17. XLVI School "Physics of Condensed States-2012" of Petersburg Institute of Nuclear Physics, March 12–17, 2012, Sankt-Petersburg, Russia;
18. 12th European Meeting on Ferroelectricity (EMF 2011), June 26 – July 1, 2011, Bordeaux, France;
19. 2nd International Conference on Nanomaterials Science and Mechanical Engineering (ICNMSME2019), University of Aveiro, Portugal, July 9–12, 2019;
20. Scanning Probe Microscopy. Russia-China Workshop on Dielectric and Ferroelectric Materials (SPM-2019-RCWDFM). Joint International Conference. Ekaterinburg, Ural Federal University, August 25–28, 2019;
21. International Symposium, dedicated to the 150 Anniversary of the Faculty of Transport and Mechanical Engineering. Section "Biomedical Engineering and Physics". Riga: RTU, October 16–18, 2014;
22. International Baltic School of Solid State Physics and Magnetism phenomena, Russia, Svetlogorsk, Kaliningrad, 11–18 August, 2012;
23. International conference "Functional Materials and Nanotechnologies" (FM&NT-2020), Lithuania, Virtual Vilnius, November 23–26, 2020;
24. International Conference on Nanomaterials Science and Mechanical Engineering, University of Aveiro, Portugal, July 16–18, 2018;
25. 4th International Conference on ElectroChemistry, Rome, Italy, June 11–12, 2018;
26. VII International Conference "Mathematical Biology and Bioinformatics", IMPB, RAS, Pushchino, Russia, October 14–19, 2018;
27. IV International Conference "Mathematical Biology and Bioinformatics", IMPB, RAS, Pushchino, Russia, October 14–19, 2012.

The results have been published in the following conference proceedings

1. Engineering of the Hydroxyapatite Cell Adhesion Capacity. Dekhtyar Yu., Bystrov V., Bystrova A., Dindune A., Katashev A., Khlusov I., Palcevskis E., Paramonova E., Polyaka N. N., Romanova M., Sammons R., Veljović D. International Symposium on Biomedical Engineering and Medical Physics. IFMBE Proceedings. 2013. Vol. 38. pp. 182–185. – DOI: 10.1007/978-3-642-34197-7_48. (Impact factor = 0.27 (2020)).
2. Computational study of hydroxyapatite properties and surface interactions. Bystrov V., Costa E., Santos S., Almeida M., Kholkin A., Dekhtyar Yu., Bystrova A. V., Kopyl S., Paramonova E. V. IEEE Conference Publications. From "Applications of Ferroelectrics" held jointly with 2012 European Conference on the Applications of Polar Dielectrics and 2012 International Symposium "Piezoresponse Force Microscopy and Nanoscale Phenomena in Polar Materials" (ISAF/ECAPD/PFM). 2012. pp. 1–3. DOI: 10.1109/ISAF.2012. 6297766. http://ieeexplore.ieee.org/ xpl/mostRecentIssue.jsp?punumber=6279558. – (Impact factor = 10.694 (2018)).
3. Interactions of charged and surface modified hydroxyapatite with living cells. Bystrov V.S., Bystrova A. V., Dekhtyar Yu., Costa M. E. V., Almeida M. M., Santos C., Kopyl S., Paramonova E. V., Kholkin A. L. Proceedings of the 9th International Conference on Bionics and Prosthetics Biomechanics and Mechanics Mechatronics and Robotics (ICBBM 2013). Riga: LABPOTO, 2013. pp. 221–228.
4. Computational study of Hydroxyapatite nanostructures, properties and its surface interactions with various species in different conditions. Bystrov V.S., Coutinho J., Costa E., Dekhtyar Yu., Bystrova A. V., Santos C., Almeida M., Kopyl S., Bystrova V. V., Paramonova E. V. Proceedings of the 4th International Conference on Mathematical Biology and Bioinformatics. Moscow: MaxPress, 2012. pp. 26–27.
5. Modeling the properties of monoclinic ordered hydroxyapatite. Bystrova A. V., Dekhtyar Yu. D., Paramonova E. V., Bystrov V. S. In the book: Mathematical Biology and Bioinformatics: reports of the V International Conference (Pushchino, October 19–24, 2014). Ed. Lakhno V. D. Volume 5. M.: MAKS Press, 2014. pp. 38–39. (RSCI, in Russian).
6. Modeling of defects in the structure of hydroxyapatite. V. S. Bystrov, R. Pullar, J. Coutinho, Yu. Dekhtyar, A. V. Bystrova, E. V. Paramonova, L. A. Avakyan. In the book: Mathematical Biology and Bioinformatics: Reports of the VI International Conference. October 16–21, 2016, Pushchino. Edited by Ph.D. V. D. Lakhno. Volume 6. M.: MAKS Press, 2016. p. 136. (RSCI, in Russian).
7. Defects in hydroxyapatite: structure and properties, calculations from the first principles Bystrov V. S., Paramonova E. V., Avakyan L. A., Coutinho J., Bystrova A. V. Reports of the International Conference "Mathematical Biology and Bioinformatics" Ed. V. D. Lakhno. Volume 7. Pushchino: IMPB RAS, 2018. Article No. e47. DOI: 10.17537 / icmbb18.1 (RSCI, in Russian).
8. Computational modeling and studies of hydroxyapatite with defects of the oxygen vacancy type providing its photocatalytic activity Bystrov V. S., Coutinho J., Avakyan L. A., Bystrova A. V., Paramonova E. V., Dekhtyar Yu. D. Proceedings of 4th

International Conference on ElectroChemistry Volume 7. Rome: Biosensors Journal, 2018. Page 98. DOI. 10.417212090-4967-C1-003.

Publications

The work results were published in 42 scientific publications, including 12 papers cited in Scopus, Web of Science; 9 papers published in leading journals with an impact factor; 8 papers published in proceedings, including proceedings with an impact factor; chapter in book. H-index: 6.

The most important publications on Thesis results

- **papers in referred (reviewed) journals:**

1. Bystrov V., Bystrova A., Dekhtyar Yu. HAp nanoparticle and substrate surface electrical potential towards bone cells adhesion: Recent results review. Advances in Colloid and Interface Science. 2017. Vol. 249. pp. 213-219. DOI: 10.1016/j.cis.20 17.05.002. (Impact Factor = 7.489, Q1).
2. Bystrov V. S., Paramonova E. V., Dekhtyar Yu. D., Bystrova A. V., Pullar R. C., Kopyl S., Tobaldi D. M., Piccirillo C., Avakyan L. A., Coutinho J. Surface modified hydroxyapatites with various functionalized nanostructures: Computational Studies of the Vacancies in HAP. Ferroelectrics. 2017. Vol. 509. pp. 105–112. DOI: 10.1080/00150193. 2017.1294436. (Impact Factor = 0.750, Q3).
3. Bystrova A. V., Dekhtyar Yu. D., Popov A. I., Coutinho J., Bystrov V. S. Modified Hydroxyapatite structure and properties: Modelling and synchrotron data analysis of modified Hydroxyapatite structure. Ferroelectrics. 2015. Vol. 475. Issue 1. pp. 135–147. DOI:10.1080/00150193.2015.995580. (Impact Factor = 0.750, Q3).
4. Bystrov V. S., Coutinho J., Bystrova A. V., Dekhtyar Y. D., Pullar R. C., Poronin A., Palcevskis E., Dindune A., Alkan B., Durucan C., Paramonova E. V. Computational study of hydroxyapatite structures, properties and defects. J. Phys. D: Appl. Phys. 2015. Vol. 48. pp. 195302-195322. DOI:10.1088/0022-3727/48/19/195302. (IF = 3.169, Q1/Q2).
5. Bystrova A. V., Dekhtyar Yu., Popov A. I., Bystrov V. S. Modelling and Synchrotron Data Analysis of Modified Hydroxyapatite Structure. Mathematical Biology and Bioinformatics. 2014. Vol. 9(1). pp. 171–182. URL: www.mathbio.org/2014/ Bystrov 9 171.pdf. (Impact Factor = 0.68).
6. Bystrov V. S., Paramonova E. V., Costa M. E. V., Santos C., Almeida M., Kopyl S., Dekhtyar Yu., Bystrova A. V., Maevsky E. I., Pullar R. C., Kholkin A. L. A computational Study of the Properties and Surface Interactions of Hydroxyapatite. Ferroelectrics. 2013. Vol. 449(1). pp. 94–101. DOI: 10.1080/00150193.2013.822774. (Impact Factor = 0.750, Q3).
7. Bystrov V. S., Paramonova E., Dekhtyar Y., Katashev A., Karlov A., Polyaka N., Bystrova A. V., Patmalnieks A., Kholkin A. L. Computational and experimental

studies of size and shape related physical properties of hydroxyapatite nanoparticles. Journal of Physics: Condensed Matter. 2011. Vol. 23. N6. pp. 065302–065312. DOI: 10.1088/0953-8984/23/6/065302. (Impact Factor = 2.711, Q1).

8. Bystrov V. S., Coutinho J., Avakyan L. A., Bystrova A. V., Paramonova E. V. Piezoelectric, ferroelectric, and optoelectronic phenomena in hydroxyapatite with various defect levels. Ferroelectrics. 2020. Vol. 559. N1. pp. 45–55. DOI: 10.1080/00150193.2020.1722005. (Impact Factor = 0.750, Q3).
9. Baltacis K., Bystrov V., Bystrova A., Dekhtyar Yu., Freivalds T., Raines J., Rozenberga K., Sorokins H., Zeidaks M. Physical fundamentals of biomaterials surface electrical functionalization. Materials. Special Issue "Recent Advances in Biocoatings". 2020. Vol. 13. N20. p. 4575. DOI: https://doi.org/10.3390/ma13204575. (Impact Factor = 3.057).

- **chapter in a book:**

1. V. Bystrov, A. Bystrova, Yu. Dekhtyar, I. Khlusov, V. Pichugin, K. Prosolov, Yu. Sharkeev. Electrical functionalization and fabrication of nanostructured hydroxyapatite coatings. - Chapter 7. In the book: Bioceramics and Biocomposites: From Research to Clinical Practice. Ed. A. Iulian. First edition. The American Ceramic Society. Publisher: John Wiley & Sons, Inc., Hoboken, New Jersey. 373 p. – pp. 149–190. 2019. ISBN: 9781119049340. Publication date: 04/15/2019.

The following bachelor thesis supervised by the author were developed on the topic of the research

1. Trone, S. High-frequency electromagnetic radiation impact on the Hydroxyapatite surface charge. Riga: [RTU], 2013, 67 p.
2. Katlapa, A. Gamma-ray influence on hydroxyapatite surface charge. Riga: [RTU], 2014, 69 p.

The Doctoral thesis contains an introduction, 3 chapters, conclusion, recommendations and 2 appendices.

INTRODUCTION

The electrical potential of the HAp surface is important in terms of biocompatibility, which is the capability of an implant to exist in harmony with tissue without causing deleterious changes [1]. When the bone implant has been inserted, the bone cells that provide regenerating of the bone tissue and compatibility with an implant should be adhered on implant's surface [2] and start to reproduce, grow, proliferate and spread on the surface coating of implants [3–6].

Artificial HAp is the most widely used material for production of bone implants [2–6, 12–16]. The molecular formula of HAp is $Ca_5(PO_4)_3OH$. The structure of HAp contains ionic bonds between calcium atoms with PO_4 groups and between calcium atoms with OH groups, covalent bonds between phosphorus and oxygen atoms in the PO_4 group and between oxygen and hydrogen in OH groups, hydrogen bonds between OH groups along the ion channel, between H atoms in OH-groups and O atoms from PO_4 groups [11].

The synthesized HAp does not have an ideal crystal structure. HAp samples used for various studies and implants production are prepared from HAp nanoparticles (NP) powder. HAp particles have different size. Therefore, they have significant curvature and unevenness of their surface, which influence electrical surface charge (polarization) [21]. This induced electrical field influences the osteoblast/osteocyte adhesion [17, 22]. Thus, HAp implant's surface properties influence the living cells' motions and adhesion to HAp surface, as well as the subsequent cell proliferation and bone tissue regeneration.

To engineer electrical surface charge, it is necessary to reconstruct the ionic – covalent and hydrogen bonds in HAp structure. One of the possible mechanisms for such surface charge formation is the charge transfer (protons' transfer through columnar HAp structure (OH-channels) and their trapping in the "frozen" states on the HAp surface) [12–14, 18, 34, 35, 40, 41, 46–49]. Another option is a charge insertion (formation of vacancies or interstitials). But there is not enough research to understand this process.

Part 1. LITERATURE REVIEW
Structural properties of HAp for controlling electrical potential of its surface

This part is devoted to the description of the structural HAp characteristics and treatment methods to engineer the electrical potential of HAp surface. The unclear and insufficiently explored aspects are formulated in Conclusion, and based on them the main goal and tasks of this Thesis work were established.

A feature of the HAp structure is OH channels. By examining OH-channels in HAp structure it is possible to understand that major contributor to HAp surface electrical potential changes is hydrogen atoms. The H atom can be transferred from/to the surface by using hydrogen bonds [12–14, 21, 22].

By applying electric field, temperature, and/or pressure, protons can propagate through this OH-channel and localize on HAp's surface. Therefore, the surface charge may change. Proton propagation is limited by internal asymmetric double-well potentials that form energy barriers.

Proton transfer depends on the concentration of hydrogen atoms (or protons) on the surface. It has been shown that the electrical potential may be engineered, for example, by hydrogenation of HAp [29, 30, 43].

The changes of HAp surface electrical potential can be produced by the defects of structural imperfection – vacancies, interstitials, etc. Potential induction depends on the crystallographic orientation of the HAp surface. Since HAp samples investigated in this Thesis are ceramic pressed from nanoparticles powder, that retain a crystalline structure at least in the immediate vicinity, the size of nanoparticles may influence the surface charge and surface homogeneity.

Part 2. THEORETICAL PART
Design of a model of crystalline HAp structures

Part 2 of the Thesis is devoted to the computational modelling of HAp structures and properties. The methods and software used to study crystalline HAp are described. The results of computational modelling of HAp structures with and without structural imperfections (O-, H-, OH-vacancy, H-interstitials, hydrogen filling unsaturated hydrogen bonds) in HAp unit cell are presented in this part as well.

The models obtained in this study allow:

1) obtaining dipole moments and polarizations of HAp structures with and without defects;
2) calculating the electron density of states (DOS) and energies corresponding to HAp defects.

It provides an opportunity to evaluate the influence of structural imperfections on HAp surface potential, to evaluate the possibilities of using OH-channel to generate point defects (vacancies and interstitials), and to decrease time and expenses for experiments.

The following steps were taken to construct the models.

1. Computational methods, which allow obtaining distribution of charges, dipole moments and polarization, energies of HAp structures and electrons' energy, were chosen. **Computational methods**, used in this Thesis, are considered in Section 2.1. The first one is based on the classical Coulomb interacting of effective atomic fixed charges with fixed positions in space – it is used for classical molecular mechanics (MM) methods. This method is used for restricted atomic-molecular cluster models in the first approximation. The second method is based on self-consistent atomic charges, which are computationally determined through the solutions of quantum-mechanical equations (Schroedinger, Hartree–Fock, etc.). In this case, atomic nuclear charges and electronic density charges distribution are used as a linear combination of the electronic molecular orbitals with different basis sets for various electronic states. This approach is used for atomic-molecular cluster models in quantum approximation and for periodic structures in density functional theory (DFT) with various approximation. Both theoretical approaches are used for all different HAp structure modelling and calculations, described in this research.
2. Software for computational modelling, which needed to be fast enough and to have a good calculation convergence, was chosen. **Software for computational modelling** is described in Section 2.2 – HyperChem (Section 2.2.1, [39]) and AIMPRO (Section 2.2.2, [32]) were used. HyperChem software (QM, semi-empirical PM3, restricted and unrestricted Hartree–Fock (RHF/UHF) approximation) was used for calculations of HAp properties for limited cluster: dipole momentum, volume, polarization, atomic charges, bond lengths and energies. AIMPRO software (QM, DFT, local density approximation (LDA)) was used for calculations of HAp properties for infinitive periodic structure: unit cell parameters, volume, atomic charges, bond lengths, electron density of states (DOS) and energies.

3. Minimal HAp clusters were constructed analogously to Posner's cluster, using hexagonal HAp unit cell, which is described in Section 2.3. The initial clusters of HAp were constructed using the common well-known experimental crystal cell parameters for HAp (obtained from CIF, Crystallographic Information File, [46]): $a = b =$ 0.946 nm, c = 0.685 nm – for hexagonal $P6_{3/m}$; and a = 0.948 nm, b = 1.896 nm, c = 0.683 nm – monoclinic $P2_{1/b}$ phases, respectively. The OH dipoles form a columnar structure in the HAp crystal (OH-channel). Repeating this unit cell in 3 dimensions (Fig. 1.1, Part 1), HAp clusters with any size as well as infinite crystal structure, used for DFT calculations in AIMPRO, can be constructed. The minimal HAp cluster [13] is shown in Fig. 2.1. For this structure quantum-chemical calculations were made using PM3 method in RHF/UHF approximation.

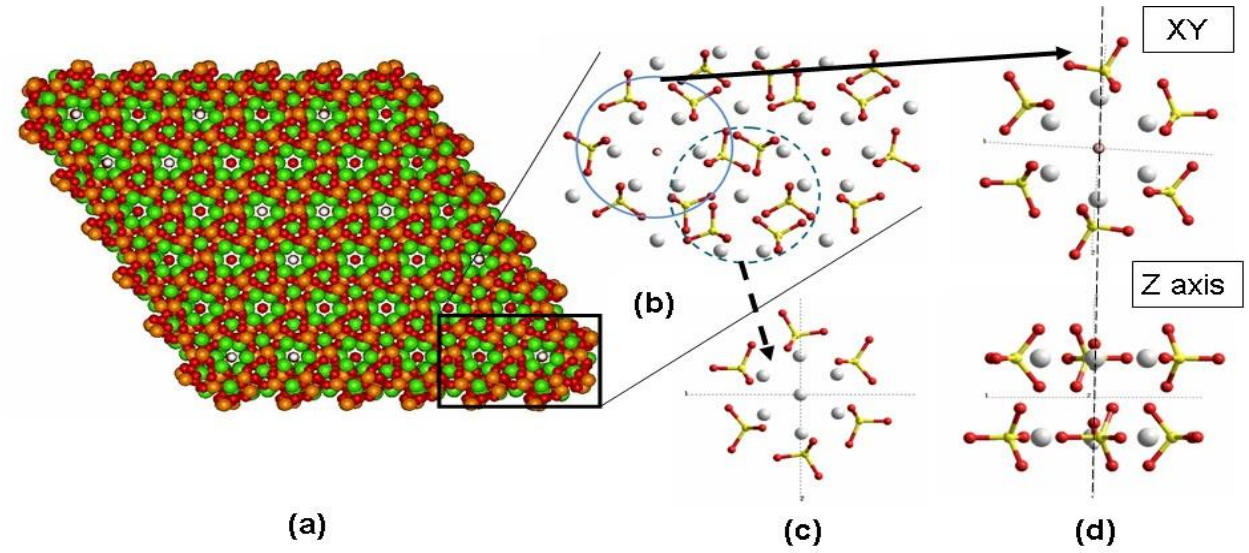

Fig. 2.1. Schematic of cut-off presentation and formation of two kinds of minimal HAp clusters: (a) biggest cluster with 36 OH channels (constructed in [34-35]); (b) cut-off procedure of minimal clusters; (c) Posner cluster (PC); (d) minimal sized HAp cluster [13] with only one OH channel.

4. The influence of protons on HAp properties is estimated and discussed in Section 2.4. The descriptions of simulations of H-vacancy inside OH-channel and saturated hydrogen bonds in minimal HAp cluster are presented in this Section as well. Quantum-chemical calculations for minimal HAp cluster allow obtaining each charge distribution, the dipole moment D (with components D_x, D_y, D_z) of this cluster and its polarization (with component P_z along the axis of the ion channel).

Table 2.1. Computed data variations of HAp minimal cluster [13]

Type of HAp cluster	Volume, Å^3	D total, Debye	D_z, Debye	Polarization P, C/m^2	P_z, C/m^2	Total cluster energy E, eV	E_g min, eV
HAp min	345.69	11.549	5.580	0.1114	0.054	–11.6506	5.3649
HAp min with 6 H atoms filling unsaturated hydrogen bonds	361.30	10.602	6.332	0.0979	0.059	–11.7947 (–0.144)	4.4603
HAp min with one H vacancy	343.02	15.999	15.496	0.1556	0.151	–11.6234 (+0.027)	5.0159

The minimum HAp cluster is characterized by:

- its dipole moment and polarization, which form an asymmetric electric field and potential distribution in the surrounding space;
- how hydrogen atoms (protons) affect the dipole moment of HAp.

The dipole moments in these HAp NPs are directly oriented in relation to the OH-channel and, therefore, (similar to spontaneous polarization in ferroelectrics) form a polarized ordered structure. In this case, the electric field lines are torus and oriented in the opposite direction to the polarization.

Cluster size (Subsection 2.4.1), **orientation and shape** (Subsection 2.4.3) influence the HAp properties. EWF (electron work function or φ) depends on the size of the HAp cluster. These results are confirmed by experiments (Fig. 2.2) [13, 49].

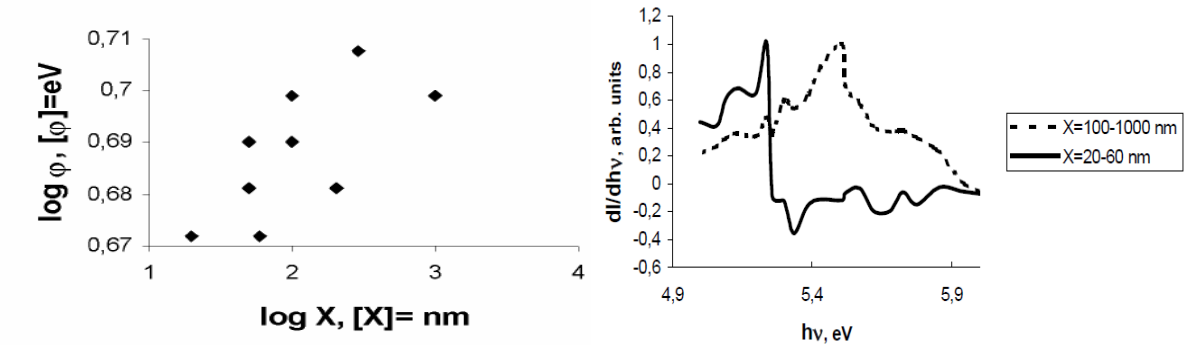

a) b)

Fig. 2.2. a) Increment of EWF value with increase of HAp NPs size [13, 49]; b) shift of the PE emission peak with the rise of HAp NPs size.

The polarization values calculated in the model are not large (about 0.005–0.010 C/m^2), in comparison to the values in the case of applied electric field ~0.1 C/m^2 [12, 36]. But this polarization is essential for HAp NP structure, because it appears and exists as self-polarization or as a spontaneous self-organized polarization. Such a process is similar to the known ordered dipole momentum and spontaneous polarization in the ferroelectrics. This polarization leads to the existence of an electric field inside and outside the HAp cluster. This internal electric field shifts the entire energy band structure of the HAp NPs. **Changes of HAp energy band structure depending on the cluster size** are considered in Subsection 2.4.2. It is shown that the largest shift evidently influences surface energy levels. Consequently, the corresponding EWF changes with size variation [13, 49]. For example, if the size of NP changes from ~20–60 nm to ~100 nm, EWF value changes by ~0.28–0.60 eV. A similar change is observed in the experiment (Fig. 2.2 a), in which the emission current derivative shifts by 0.3 eV [13, 49].

5. HAp structures with various defects are constructed to obtain data about dipole moment, polarization, the total energy for HAp structures with defects. HAp structures with various defects are described in Sections 2.5 and 2.7.

   As the goal of this work is to analyse the possibility of using OH-channel to generate points defects, which influence electrical potential of HAp surface, the models of

corresponding HAp unit cell with investigated defects were considered: O-, H- and OH-vacancy inside OH-channel, H- interstitial inside OH-channel; H-insertion on unsaturated hydrogen bonds.

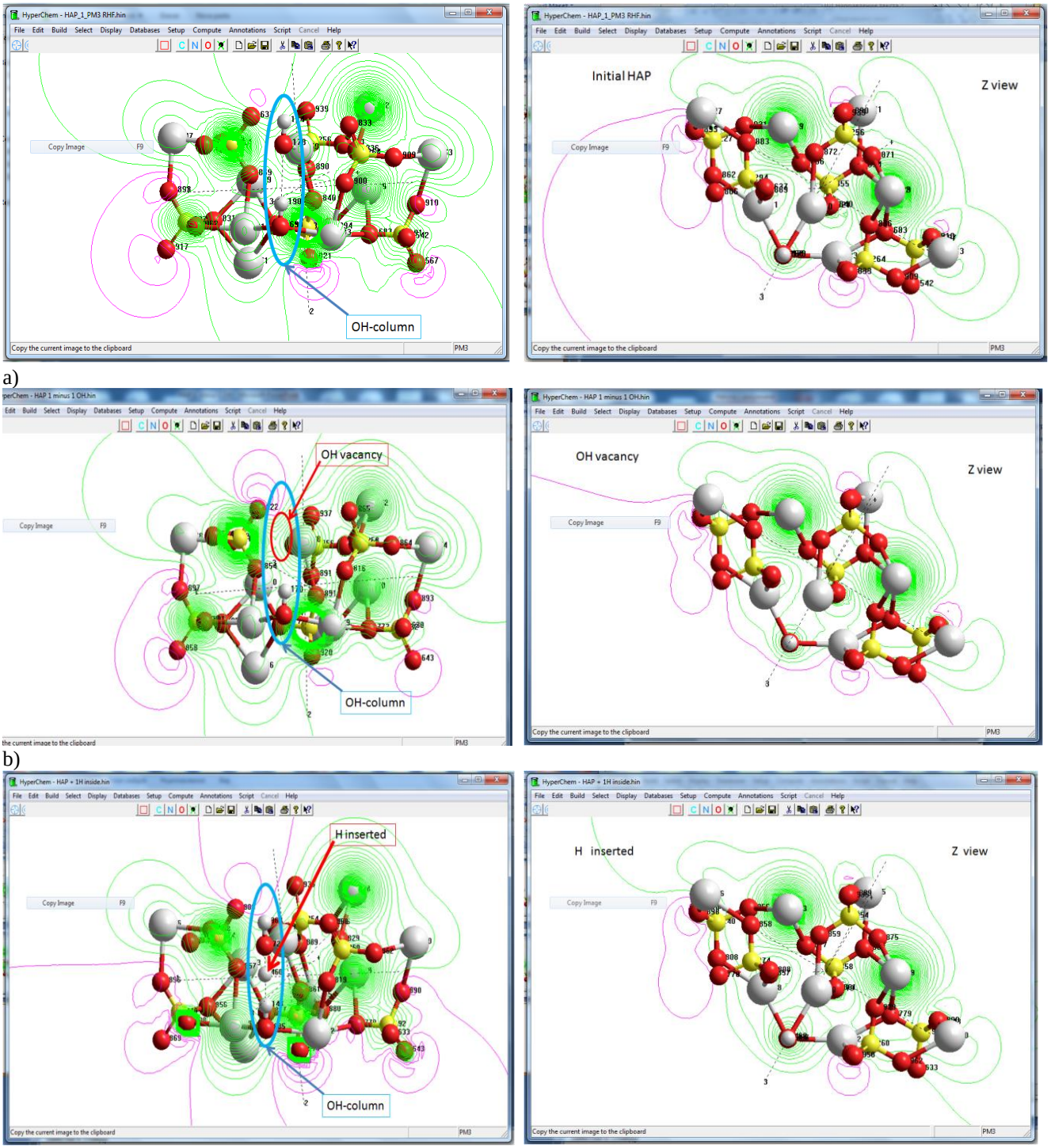

Fig. 2.3. Electrostatic potential distribution in HyperChem workspace – *Y* and *Z* views: (a) for initial defectless hexagonal HAp unit cell; (b) HAp unit cell with one OH-vacancy in OH-channel; (c) HAp unit cell with one H inserted in OH-channel.

Based on computed data of defectless HAp minimal cluster (Section 2.3) and DFT LDA (Subsection 2.2.2), the initial defectless HAp unit cell with 44 atoms was modified and the models of several defects in HAp structure were calculated [28, 45]. The simulation of these defects was done on the base of modified HAp unit cell (42 and 43 atoms for vacancies and 45 and 46 atoms for insertion of additional interstitial [28, 33]). The models are presented in Fig. 2.3.

Fig. 2.3 shows obtained electrostatic potential distribution for initial defectless hexagonal HAp unit cell (2.3 a); HAp unit cell with one OH-vacancy in OH-channel (2.3 b), and HAp unit cell with one H inserted in OH-channel (2.3 c).

6. Calculation of DOS for all these structures was done and described in Section 2.5. Subsection 2.5.1 provides data on changes of the forbidden band of the HAp crystals with defects. As an example, the scheme of the computed DOS for defectless HAp structure in comparison with HAp cell with OH-vacancies [28] is presented in Fig. 2.4.

The DOS structure for the defectless hexagonal HAp consists of several peaks (A, B, C and D) in the valence band (Fig. 2.4, upper). There are deep levels below the valence band.

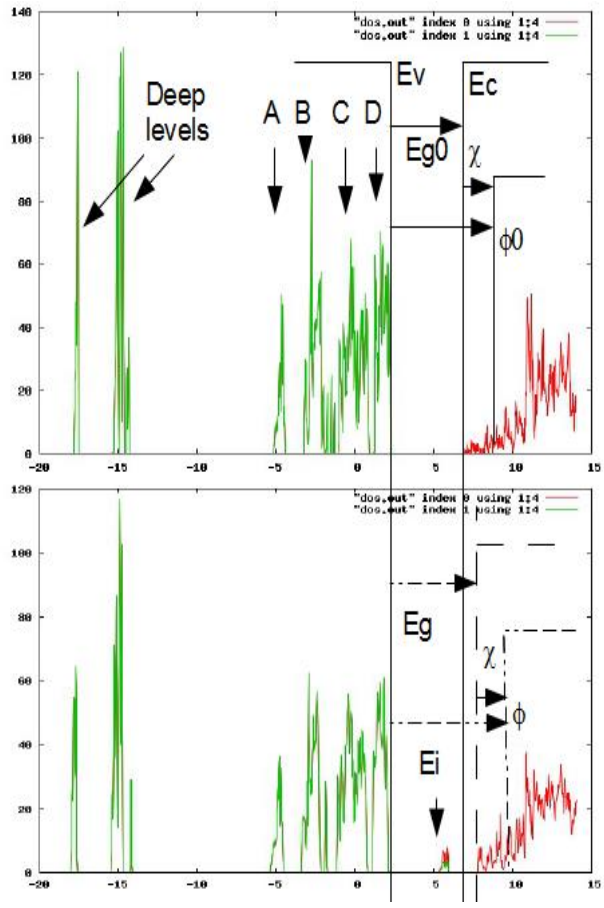

Fig. 2.4. The density of states (DOS) for defectless HAp hexagonal structure (upper image) and HAp with one OH-vacancies per one unit cell (lower image). Here A, B, C & D are the usual levels for HAp, reported in similar works [28, 45].

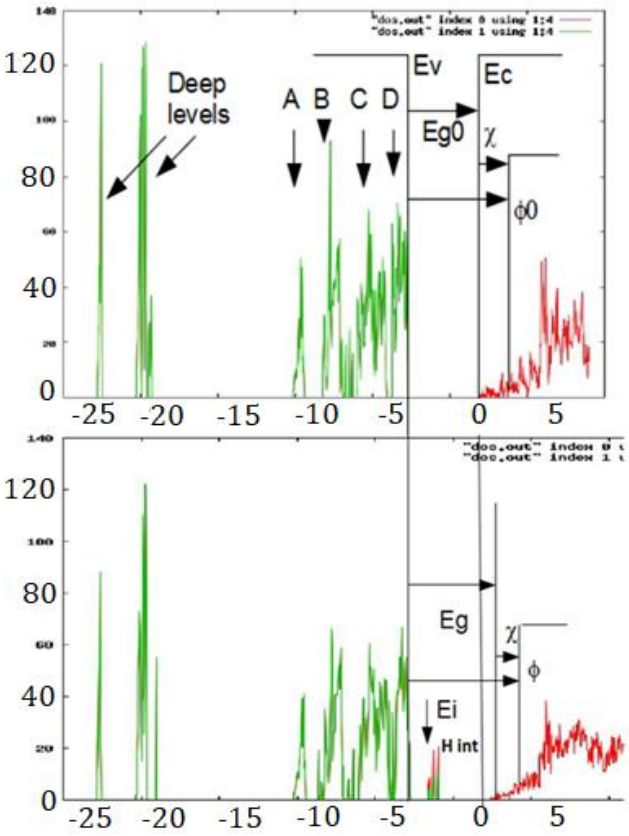

Fig. 2.5. DOS for defectless HAp hexagonal structure (upper image) and DOS with one H-interstitial in the OH channel between two OH groups in the HAp hexagonal unit cell (lower image), a local level *Ei* (H int) is induced in the forbidden zone, which is characterized by energy $E_i \approx E_v$ + (1,20–1,75) eV.

Figure 2.4 (bottom image) shows DOS of HAp with OH-vacancy that induce local energy levels in the forbidden band [28]. Figure 2.5 shows DOS of HAp with H-interstitial in the OH channel, that also induces local energy levels in the forbidden band.

Here and below the following denominations are used in this work: E_{g0} and φ_0 as the forbidden band and electron work function for HAp without defects, E_g and φ – for all cases with defects.

For the DOS peaks in the valence band E_v is the top of the valence band, E_c is the bottom of the conductive band. Taking the denominations into account, $E_g = E_c - E_v$, $\varphi = \chi + E_g$ (χ – affinity), but changes of φ influence HAp defect $\Delta\varphi = \varphi - \varphi_0$, or $\Delta\varphi = E_g - E_{g0} = \Delta E_g$, if χ is constant. Horizontal arrows in Fig. 2.4 show the direction of the electron excitation, other arrows identify levels in valence bands of HAp.

All obtained DOS characteristics of HAp structures with investigated defects are presented in Table 2.2 [28]. Average computational error is ±0.05–0.10 eV.

Table 2.2. DOS characteristics of HAp structures [28]

Defect type	Lattice parameters, Å	Change of total energy ΔE from defectless HAp, %	E_g, eV	Change of E_g from defectless HAp, eV	Local levels, measured from the top of valence band ($E_i - E_v$), eV	Local levels, measured from the bottom of conductive bands ($E_c - E_i$), eV
HAp without defects	a = 9.4732 c = 6.9986	–	4.6	–	–	–
Vacancy H	a = 9.4537 c = 6.9916	–0.15	4.92	+0.32	½ occupied 0.1	4.82
Vacancy O	a = 9.4539 c = 7.0028	–3.57	5.15	+0.55	½ occupied 0.1	5.05
Vacancy OH	a = 9.4883 c = 7.0018	–3.71	5.49	+0.89	½ occupied band 3.11–3.82 with peaks 3.40 3.53 3.66	band 2.38–1.67 peaks 2.09 1.96 1.83
Interstitial H	a = 9.5013 c = 6.9842	0.10	5.12	+0.52	½ occupied peaks 1.20 1.45 1.75	peaks 3.92 3.67 3.37
2 H atoms filling unsaturated H bonds	a = 9.5228 c = 7.0001	0.21	4.63	+0.03	1.71 0.79	peaks 2.92 3.74

Comparing these data, it is clearly visible that OH-vacancy mostly influences electrical HAp properties.

Local levels inside the HAp forbidden band are induced by the presence of structural imperfection. Due to the fact that they may be electron donors and acceptors, they are recombination centres. It means that photoluminescence (PL) can be observed after preliminary electron excitation by phonons from the valence band to the conductive band.

Influence of H^+ captured by unsaturated bonds in HAp unit cell on its properties is considered in Subsection 2.5.2. Calculations made by the DFT method in the local density approximation (LDA DFT) [28] have shown that the capture of two hydrogen atoms on existing two unfilled left bonds per one unit cell of hexagonal HAp leads to the appearance of two additional levels inside the forbidden band E_{i1}, E_{i2} (measured from the bottom of the conductive band), which are both electron acceptors and recombination centres. Thus, such levels could be detected using PL (when the previously excited electron trapped from the conductive band to those local levels).

Part 3. EXPERIMENTAL PART
Experiments to engineer the HAp surface charge

3.1. Introduction

The aim of this part is to experimentally confirm the effect of defects in HAp structure on its surface electrical potential shown in theoretical estimations (Part 2).

The idea of the experimental part is to generate defects in the HAp sample surface layers, thereby to change HAp sample surface charge and, therefore, the potential. The energy bands structures of investigated samples were constructed based on measurements and compared with the results of the theoretical part.

The following tasks are set in the experimental part:

1) to choose HAp treatment methods for defect generation (Section 3.3);
2) to choose research methods (Section 3.4);
3) to compare the results obtained in the experiments with the theoretical data (Section 3.7).

3.2. Characteristics of investigated native samples of HAp

The pressed ceramic nanopowder HAp samples were used for the research in this work. The samples consist of HAp NPs clusters (~100 nm sizes), which are formed by combining small NPs (~20 nm) [13, 18].

The samples have the following characteristics:

1) the crystal structure of the samples corresponding to hexagonal HAp [18];
2) average size of the ceramic grains (300 ± 100) nm [13, 20];
3) porosity within 17...26 % [18]; dimensions of canals: 0.2...6.0 μm width, 25...85 μm length [18];
4) cylinder shape tablets with a diameter of 5 mm and thickness of 2 mm;
5) chemical composition: Ca/P =1.67 [48].

3.3. Treatments applied to HAp samples

The surface charge can be changed by charge insertion or charge transfer. The charge transfer is possible by inserting an atom (H) into OH-channel. The charge insertion is possible by the formation of OH-, O- or H- vacancies. The treatment types used to generate defects are considered in Table 3.1.

Table 3.1. Treatment types and induced defects

Defect type	**Treatments type**
Vacancy OH	Annealing 500–900 °C [20]
Vacancy O	Gamma-ray irradiation [38]
Vacancy H	
Interstitial H	Hydrogenation [29] + MW irradiation

Annealing

The following parameters were used during HAp samples' annealing:

- pressure: 0.001 00–0.001 15 Pa;
- temperature: 542–546 °C;
- heating rate: 15 °C/min;
- annealing time: 30 minutes;
- cooling down to room temperature.

Hydrogenation

The following parameters were used during HAp samples' hydrogenation:

- temperature: 23 °C;
- pressure of hydrogen: (60 ± 2) atm;
- hydrogenation time: 6 hours.

Microwave irradiation

A SAMSUMG microwave oven was used with the following settings:

- power: 800 W;
- working time: 6.5 minutes.

Gamma-ray irradiation

Irradiation of HAp samples were done after annealing. A linear accelerator VARIAN CLINAC was used with the following settings:

- photon energy: 18 MeV;
- the dose rate: 1000 MU/min;
- the ionizing radiation dose: 10 Gy;
- distance from the radiation source to sample: 1 m;
- radiation field: 10 cm × 10 cm.

3.4. Research methods

For measurements of HAp samples, non-contact measurements were preferred, so as not to affect the surface charge.

Threshold PE emission spectroscopy was used to register the electrical potential of HAp sample surface and DOS changes. This allows measuring the output of electrons, which in the case of semiconductors and dielectrics is directly related to the surface charge.

Photoluminescence emission and synchrotron excitation spectroscopy methods were used for the study of deep energy levels and for the study of the peculiarities of interface interactions and properties in nanosized composed samples [27] (Subsection 3.4.4).

Measurements of PE spectra were done by irradiating the HAp sample surface with a monochromatic beam, changing the wavelength of photons from 200 nm to 270 nm with step 0.5 nm (wavelength changes by speed 0.5 nm/s). The diameter of the light beam from monochromator on the studied surface was equal to 0.2 mm. The measurement temperature in

the laboratory room is 22.5 ± 2.5 °C. Measurements were made under a vacuum of 0.0066 Pa or less. The voltage to the secondary electron multiplier cathode is 300 V, the supply voltage is 3.5 kV.

The luminescence properties of HAp in the UV-VUV spectral range were studied with pulsed synchrotron radiation from the DORIS III storage ring. Luminescence of HAp samples happens due to the recombination of electrons and holes on additional energy levels within the forbidden gap. The maximum intensity of PL was obtained at 300 K temperature and 180 nm wavelength of electron excitation during initial measurements. Thus, those parameters were chosen for recording emission spectra.

The experimental parameters were as follows:

- PL excitation wavelength was between 333 nm and 80 nm with a resolution of 0.3 nm;
- PL range of HAp samples was 200 nm to 800 nm;
- the temperature at which the measurements were made was 10 K, 300 K;
- the spectral resolution of the analysing monochromator was 11 nm.

When the normalization of the graphs to a maximum was carried out, a small structure was observed at 90 nm. This can be explained by the excitation of electrons from the deep levels.

The equipment for measuring the PL spectra is described in Subsection 3.4.6.

3.5. Course of the experiments

To prove theoretical expectations and to provide optimal technological regime to produce high- quality HAp for implantation, it was necessary to answer two questions: how HAp retains its properties for a relatively long time; how HAp changes after different applied influences.

To understand how HAp retains its properties for a relatively long time, PE emission spectra was measured on the initial HAp samples. Then the HAp samples were annealed and, after cooling to room temperature, their PE spectra were remeasured. The PE spectra of HAp samples were measured several times again during a few weeks.

To understand how HAp changes after different applied treatments, a treatment sequence was developed (Fig. 3.1).

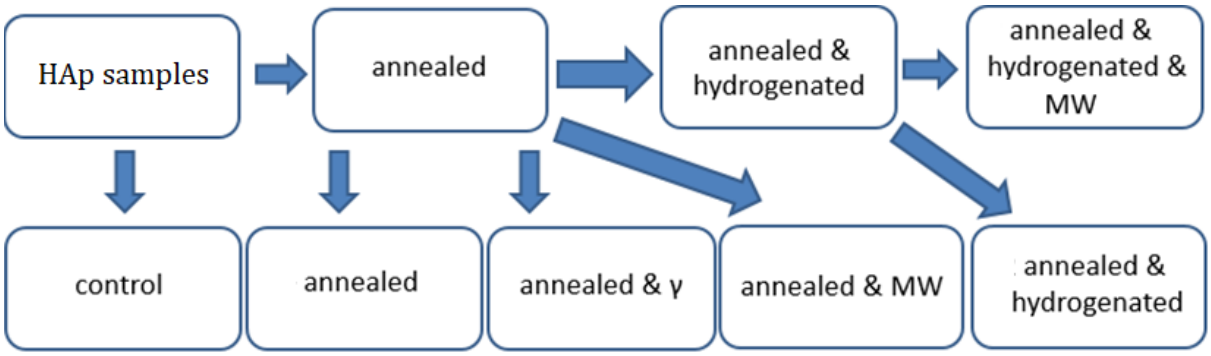

Fig. 3.1. Scheme of applied treatments on HAp samples.

Measurements of one group of samples were done during one day. The samples were kept in a plastic container, separately one from another in a dark shelve, at the same room conditions where PE measurements were done.

For PL measurements, samples were sent to Deutsches Elektronen-Synchrotron (DESY). The applied measurements and methods are summarized in Table 3.2.

Table 3.2. Total measurements and treatments on HAp samples

Group of samples	PE emission	Anne-aling	PE emission	Hydro-genation	MW irradiation	Gamma-ray irradiation	PE emission	PL	PE emission
1	+	+	+	+			+		+
2	+	+	+	+			+	+	+
3	+	+	+	+	+		+	+	+
4	+	+	+	+	+		+		+
5	+	+	+		+		+		+
6	+	+	+		+		+	+	+
7	+	+	+				+	+	+
8	+	+	+			+	+	+	+
9							+	+	+
10	+	+	+						+

The PE emission spectra of these samples were measured periodically, within two years to control HAp surface charge stability.

3.6. Methods of data processing

3.6.1. PE emission spectra processing

In the case of a pure crystal, during PE emission electrons are excited from the valence band, i.e. overcome $E_g = E_c - E_v$; and plus, they have to go out to the vacuum level, i.e. electron affinity "χ": $\varphi = E_g + \chi$. Because, as it was discussed in Subsection 1.4.2, in HAp $\chi << E_g$, $\varphi \approx E_g$. In this case, the spectrum has only one straight part, which is explained by the existence of forbidden band without any additional level from defects inside.

Recent studies and calculations by various methods of the DFT [24–26, 28] have shown that in the presence of a defect in a crystal unit cell the magnitude of the electron work function changes in comparison to the work function of a pure crystal. In the modelled HAp structure there are idealized situations (with ideal crystal lattice unit), while in real HAp structures the crystal is not ideal and has several deviations due to atomic position fluctuations. It leads to local changes in electron band structure, experimentally observed as average value of EWF as the sum of EWF values of many crystal lattice units. These changes could be seen in the comparison of computed values of the E_g energies for models of unit cells with defects (Part 2, Table 2.2) with EWF values, obtained from experimental data. So, in a more complicated case – when there are structural imperfections inside the HAp sample – the photoelectrons can be excited from these additional levels inside forbidden band and the value of EWF changes (Part 2). Altogether all these processes could be described by very complex and complicated statistical models.

As the real sample is usually non-uniform, one value of EWF can be registered from one group of unit cells with the same type of defects, and another – from another group of unit cells with different type of defects (if it is possible to determine on the spectra just one type of defects in the sample, the designation EWF is used for this case; if there are two or three – additional designations "energy barrier A1" and "energy barrier A2" are used). Since the recorded intensity curve is the total record from all the emitted particles, in general, all these components contribute to the total intensity curve. In this case the spectrum has more than one straight part (Fig. 3.2). It is necessary to use all of these values, and based on them it is possible to construct energy zone diagrams for further analysis of HAp structure.

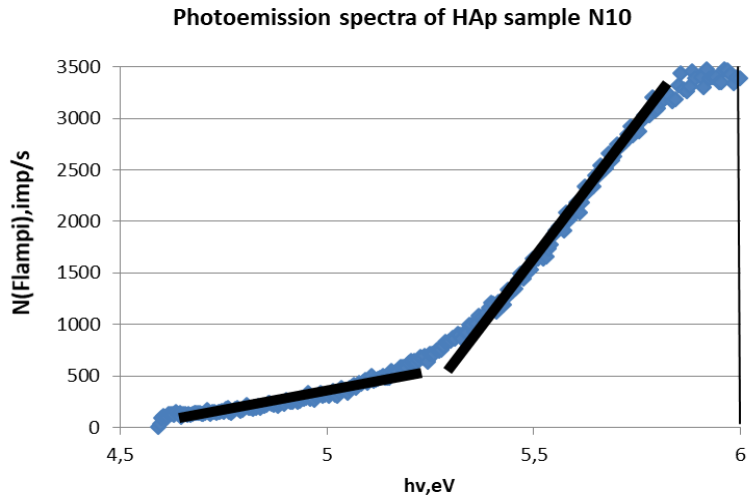

Fig. 3.2. Example of PE spectra of HAp sample with EWF variations, corresponding to two different types of cells with defects.

The values of the electron work function φ were estimated with an error of less than ±0.04 eV [13, 28]. It is comparable with the error in calculation of the density of electronic states (DOS) data in this work is ±0.05 eV [28].

3.6.2. Construction of electronic band structure diagrams

As the additional levels within the forbidden band can be shown by electronic band structure diagram (EBSD), they also were constructed for each sample to analyse the obtained PE spectra of HAp samples before and after annealing.

The EBSD has the following parameters: EWF – electron work function, E_a – energy values of additional energy levels within band gap (energy barrier A1), χ – an affinity.

The most typical EBSD is shown in Fig. 3.3.

The EBSD shows that, in general, just affinity is changing a lot and all other parameters change to a much smaller extent.

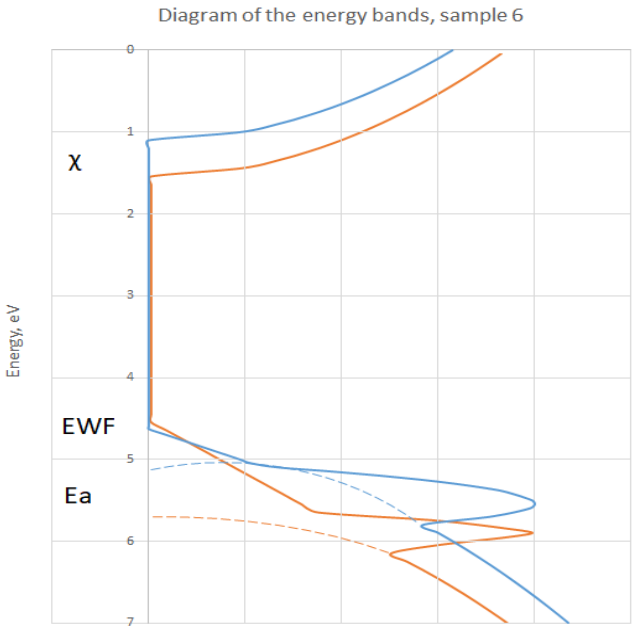

Fig. 3.3. EBSD of sample N6. Red line – before annealing and blue line – after annealing. E_a – energy barrier A1, χ – an affinity.

3.6.3. PL spectra processing

The PL graphs represent the PL luminescence intensity depending on the energy of the emitted photons (Fig. 3.4).

The maximum PL intensity is at the energy corresponding to the local energy level (2.95 eV from the bottom of the conductive band).

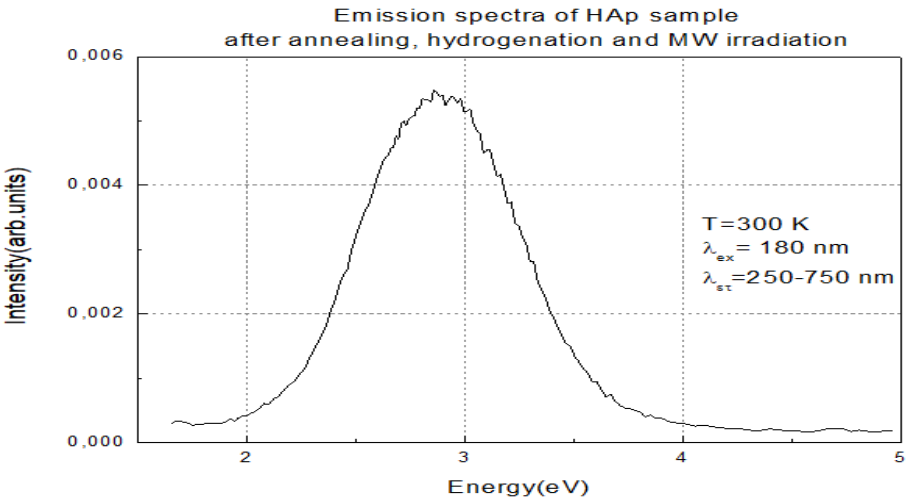

Fig. 3.4. Example of graph built in Origin 8 program.

3.7. Results of experiments and discussion

In Section 3.7, the results of HAp sample measurements are presented to answer the question how long HAp retains its structural changes and following physical properties.

To change initial HAp structure and to form defects in it, the native samples were annealed under the condition described in Section 3.3. To control the existence of produced

defects within time, PE emission spectra of these annealed HAp samples and also group of non-annealed HAp samples were measured within 2 years.

3.7.1. Stability of induced defects in HAp samples

Looking at the EWF measurements (Subsection 3.6.2) the HAp samples show no significant changes within the time span of at least 14 months (Fig. 3.5).

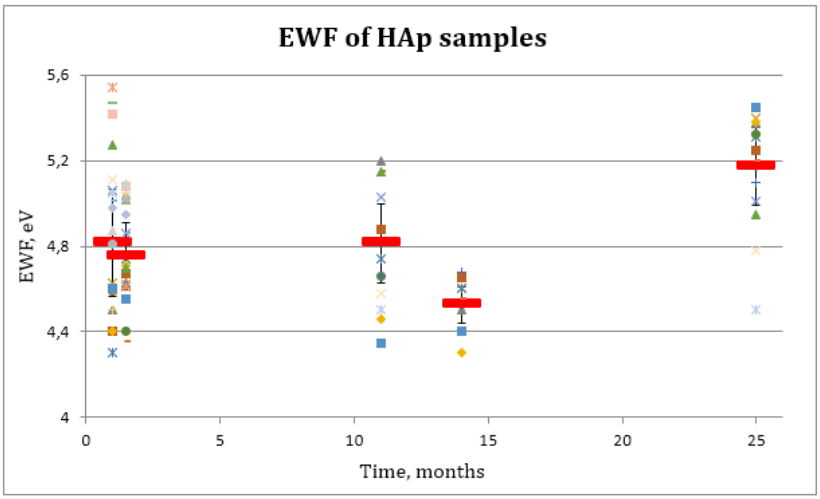

Fig. 3.5. EWF values of HAp samples in time.

It is necessary to note that the 1st and 2nd data sets of EWF were obtained on the same day, but they are represented with a one-month gap in the graph for a better overview. The 1st one is values of EWF of HAp samples before annealing and the 2nd one – after annealing.

According to the methodology (Fig. 3.2) and using experimental data, the EWF of HAp samples were calculated. The presence of defects in the samples was determined according to the calculated data of the EWF (Section 2.2, Table 2.2). All samples were sorted according to the values of EWF corresponding to the identified defects (Table 2.2).

1. Native samples are divided into groups:
    - defectless samples (6.7 % from the total amount of samples);
    - samples with saturated hydrogen bonds and H-vacancies;
    - samples with saturated hydrogen bonds and with O-vacancies or H-interstitials;
    - samples with saturated hydrogen bonds and with OH-vacancies;
    - samples with saturated hydrogen bonds and with H- and O-vacancies or H-interstitials;
    - samples with H-vacancies;
    - samples with H-vacancies and O-vacancies or H-interstitials;
    - samples with O-vacancies or H-interstitials;
    - samples with OH- and O-vacancies or H-interstitials;
    - samples with OH-vacancies.
2. Annealed samples separated by groups:
    - samples with H-vacancies and saturated by H bonds (transformed from defectless HAp samples);

- samples with O-vacancies and saturated by H bonds (transformed from defectless HAp samples);
- samples with O-vacancies and saturated by H bonds transformed from samples with H-vacancies and saturated by H bonds;
- samples with H-vacancies and saturated by H bonds, which were samples with H-vacancies and saturated by H bonds before annealing as well but had a different value of EWF;
- samples with O-vacancies and saturated by H bonds, which were samples with O-vacancies or H-interstitials and saturated by H bonds before annealing as well but had a different value of EWF;
- samples with OH-vacancies and saturated hydrogen bonds transformed from samples with O-vacancies or H-interstitials and saturated hydrogen bonds – annealing leads to knockout of hydrogen;
- samples with H-vacancies and saturated by H bonds transformed from samples with OH-vacancies and saturated by H bonds – annealing leads to knockout of oxygen;
- defectless samples transformed from samples with OH-vacancies and saturated by H bonds;
- samples with O-vacancies and OH-vacancies transformed from samples with H- and O-vacancies or H-interstitials and saturated by H bonds;
- samples with OH-vacancies and saturated by H bonds transformed from samples with H- and O-vacancies or H-interstitials;
- samples with O-vacancies and H-vacancies, which were samples with O-vacancies or H-interstitials and saturated by H bonds before annealing as well but had a different value of EWF;
- samples with O-vacancies and OH-vacancies transformed from samples with H-vacancies;
- samples with O-vacancies and OH-vacancies transformed from samples with O-vacancies or H-interstitials;
- samples with O-vacancies and saturated by H bonds transformed from samples with O-vacancies or H-interstitials;
- samples with O-vacancies and H-vacancies transformed from samples with OH- and O-vacancies or H-interstitials;
- samples with O-vacancies and H-vacancies transformed from samples with OH-vacancies;
- samples with O-vacancies and OH-vacancies transformed from samples with OH-vacancies.

3. After annealing:
   - there are no samples with H-interstitials;
   - mostly there are samples with O-vacancies;

- formation of samples with saturated hydrogen bonds and H-vacancies from defectless HAp samples means that annealing leads to hydrogen atoms knockout from HAp structure and these hydrogen atoms fill unsaturated hydrogen bonds;
- samples with saturated hydrogen bonds contain H-vacancies (45.4 %), O-vacancies (36.4 %), or OH-vacancies (18.2 %);
- samples with H-vacancies contain O-vacancies (80 %) or OH-vacancies (20 %);
- samples with O-vacancies contain OH-vacancies;
- defectless samples form in 5 % of the total amount.

4. During annealing the following processes may happen:
   - hydrogen/oxygen knockout from OH-group;
   - OH-group knockout;
   - capturing of knocked hydrogen on unsaturated hydrogen bonds.

Thus, this method of data analyses also proves that annealing under chosen parameters (Section 3.3) changes the structure of HAp.

3.7.2. Influence of annealing on HAp

In accordance with the method (Subsection 3.6.1), the energy barriers for the electron exit (E_{Ai}) and EWF of HAp were measured. The defects of samples caused by annealing were identified comparing the measured values of E_{Ai} and EWF with the calculated HAp EWF values (Part 2, Table 2.2). This comparison showed the correspondence between the EWF and the type of defects. The initial samples were grouped according to the E_{Ai} values that correspond to specific type of defects in the unit cell structure (Table 3.3). Structural changes in the HAp as a result of annealing are shown in the defect reconstruction schemes (Figs. 3.6–3.11).

Table 3.3. The initial samples, grouped by the magnitude of the energy barriers for the electron exit, corresponding to specific defects

Sample group	Calculated EWF value, eV	Type of defect in the unit cell structure	Closest measured energy barrier (E_{Ai}), eV	Scheme of defect reconstruction after annealing
1	4.6	HAp without defects	$E_{A1} = 4.51 \pm 0.15$	Fig. 3.6
2	4.63	2 additional H atoms that fill unsaturated hydrogen bonds	$E_{A1} = 4.49 \pm 0.09$	Fig. 3.7
	4.92	H-vacancy	$E_{A2} = 4.84 \pm 0.06$	
3	4.63	2 additional H atoms that fill unsaturated hydrogen bonds	$E_{A1} = 4.5 \pm 0.1$	Fig. 3.8
	5.15/5.12	O-vacancy / H-interstitial	$E_{A2} = 5.20 \pm 0.04$	
4	4.63	2 additional H atoms that fill unsaturated hydrogen bonds	$E_{A1} = 4.47 \pm 0.05$	Fig. 3.9
	5.49	OH-vacancy	$E_{A2} = 5.37 \pm 0.05$	
5	4.92	H-vacancy	$E_{A1} = 4.98 \pm 0.04$	Fig. 3.10
	5.15	O-vacancy	$E_{A1} = 5.25 \pm 0.04$	
6	5.15/5.12	O-vacancy / H-interstitial	$E_{A1} = 5.06 \pm 0.04$	Fig. 3.11
			$E_{A2} = 5.23 \pm 0.04$	

In Groups 2–4, E_{A1} correlates with the values of calculated EWF of HAp without defects as well as with the values of calculated EWF of HAp with saturated hydrogen bonds. Since two E_{Ai} from the samples of Groups 2–4 were registered (Table 3.3), corresponding to different types of defects in the structure of the HAp unit cell, E_{A1} cannot correspond to HAp without defects, but shows the presence of saturated hydrogen bonds.

After annealing, the samples of Group 1 (whose initial EWF values correspond to the calculated EWF value of HAp without defects in the structure) were sorted into two subgroups according to the E_{Ai} values in the same way as the initial samples were grouped (Fig. 3.7):

- Subgroup 1 (on the left in Fig. 3.6) – samples with two E_{Ai}: the first one with an average value of 4.74 eV, which corresponds to the value of calculated EWF = 4.63 eV of HAp with saturated hydrogen bonds, and the second – 4.9 eV, which corresponds to the value of calculated EWF = 4.92 eV of HAp with H-vacancy. This means that hydrogen atoms are knocked out during annealing, and then captured by unsaturated hydrogen bonds that were originally present in the cell;
- Subgroup 2 – HAp samples with two E_{Ai}: the first one with an average value of 4.68 eV, which corresponds to the calculated value of EWF = 4.63 eV of HAp with saturated hydrogen bonds, and the second – 5.05 eV, which corresponds to the calculated value of EWF = 5.15 eV of HAp with O-vacancy.

After 11 and 14 months, the measured EWF values of the samples of the Subgroup 1 began to correspond to the calculated EWF values of HAp with saturated hydrogen bonds or without defects in the structure. After 25 months, the measured EWF values of the samples of Subgroup 1 began to correspond to the calculated EWF value of HAp with OH-vacancy.

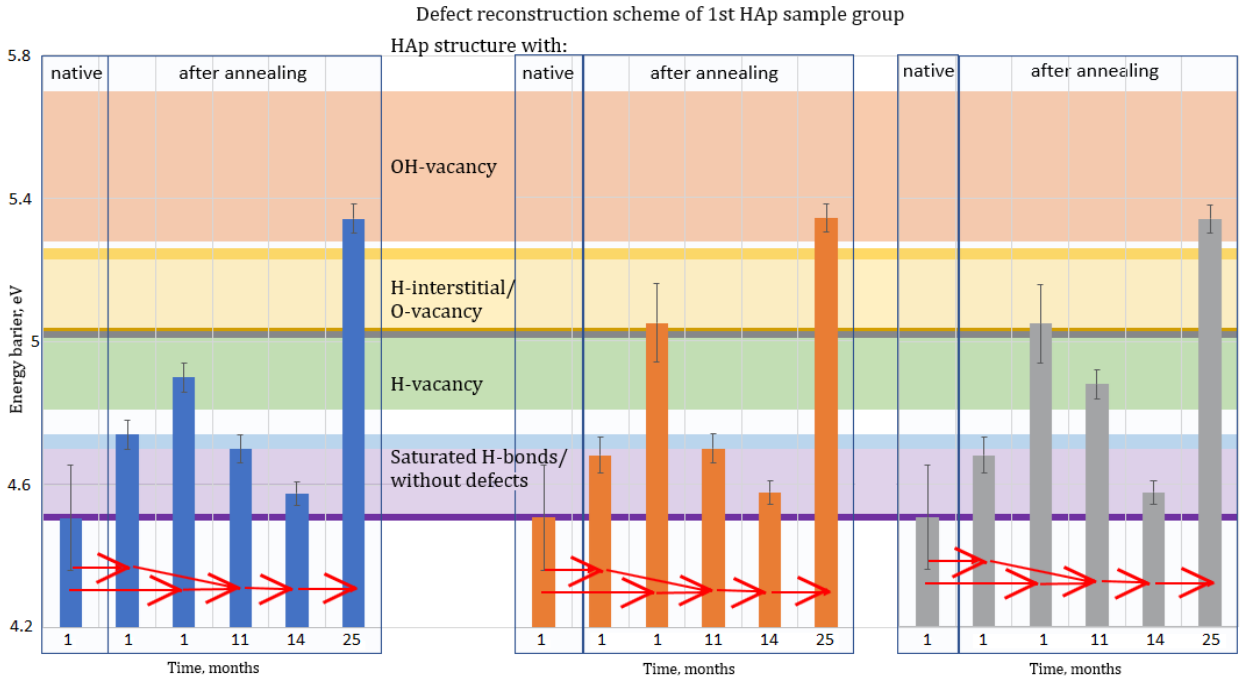

Fig. 3.6. Schemes of the defect reconstructions in samples of Group 1.

After 11 months, the measured EWF values of some samples of Subgroup 2 began to correspond to the calculated EWF value of HAp with H-vacancy (in the centre in Fig. 3.6), and measured EWF values of other samples of this group (in Fig. 3.6 on the right) – to

calculated EWF values of HAp with saturated hydrogen bonds or without defects in the structure. After 14 months, the measured EWF values of all samples of this subgroup began to correspond to the calculated EWF values of HAp with saturated hydrogen bonds or HAp without defects in the structure. After 25 months, the measured EWF values of the samples of Subgroup 2 began to correspond to the calculated value of EWF of HAp with OH-vacancy.

After annealing, the samples of Group 2 (whose initial values of E_{Ai} correspond to the calculated EWF values of HAp with saturated hydrogen bonds and H-vacancy in the structure) were sorted into two subgroups according to the E_{Ai} values in the same way as the initial samples were grouped (Fig. 3.7):

- Subgroup 1 (on the left in Fig. 3.7) – HAp samples with two E_{Ai}: the first one with an average value of 4.53 eV, which corresponds to the calculated EWF value of HAp with saturated hydrogen bonds, and the second – 5.25 eV, which corresponds to the calculated value of EWF = 5.15 eV of HAp with O-vacancy;
- Subgroup 2 – HAp samples with two E_{Ai}: the first one with an average value of 4.53 eV, which corresponds to the calculated EWF value of HAp with saturated hydrogen bonds, and the second – 5 eV, which corresponds to the calculated value of EWF = 4.92 eV of HAp with H-vacancy.

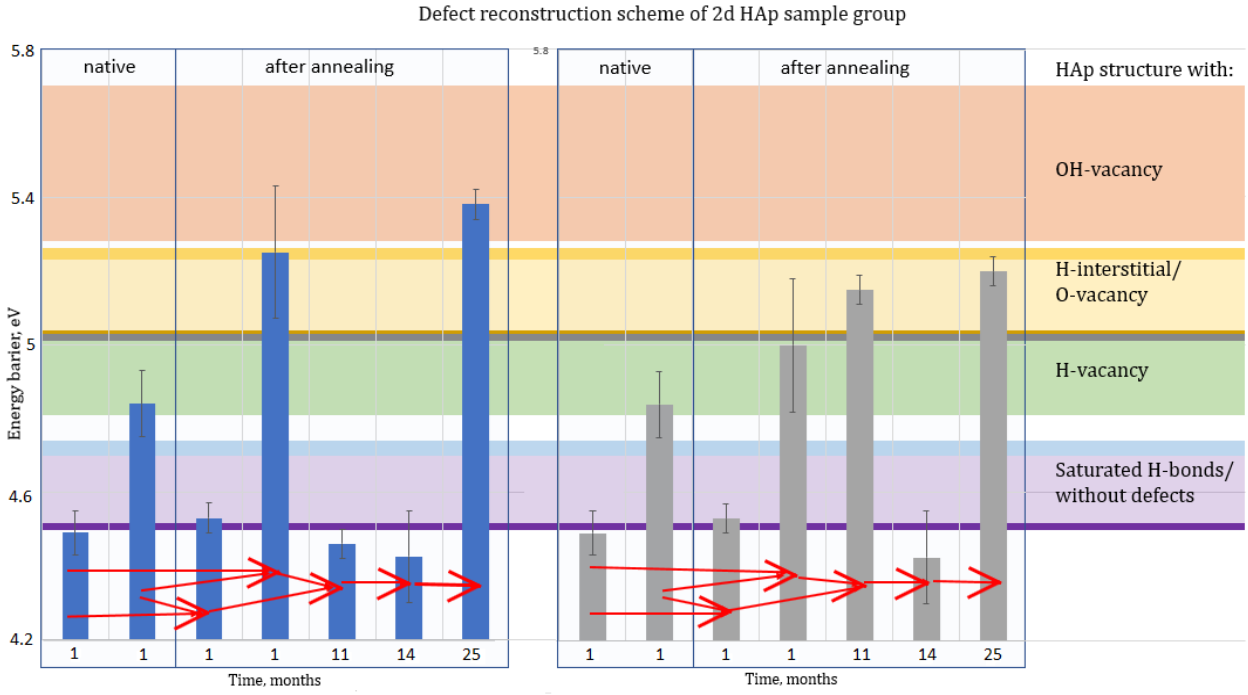

Fig. 3.7. Schemes of defect reconstructions in samples of the Group 2.

After 11 and 14 months, the measured EWF values of the samples of Subgroup 1 began to correspond to the calculated EWF value of HAp without defects in the structure. After 25 months, the measured EWF values of the samples of Subgroup 1 began to correspond to the calculated EWF value of HAp with OH-vacancy. After 11 months, the measured EWF values of the samples of Subgroup 2 began to correspond to the calculated EWF value of HAp with O-vacancy. After 14 months, the measured EWF values of the samples of Subgroup 2 began

to correspond to the calculated EWF value of HAp without defects in the structure. After 25 months, the measured EWF values of the samples of Subgroup 2 began to correspond to the calculated EWF value of HAp with O-vacancy.

After annealing, the samples of the Group 3 (whose initial E_{Ai} values correspond to the calculated EWF values of HAp with saturated hydrogen bonds and O-vacancy or H interstitial), were sorted into two subgroups according to the energy barrier values in the same way as the initial samples were grouped (Fig. 3.8):

- Subgroup 1 (on the right in Fig. 3.8) – samples with two E_{Ai}: the first one with an average value of 4.6 eV, which corresponds to the calculated EWF value of HAp with saturated hydrogen bonds, and the second – 5.3 eV, which corresponds to the calculated EWF value of HAp with OH-vacancy;
- Subgroup 2 – HAp samples with two E_{Ai}: the first one with an average value of 4.6 eV, which corresponds to the calculated EWF value of HAp with saturated hydrogen bonds, and the second – 5.2 eV, which corresponds to the calculated value of EWF = 5.15 eV of HAp with O-vacancy.

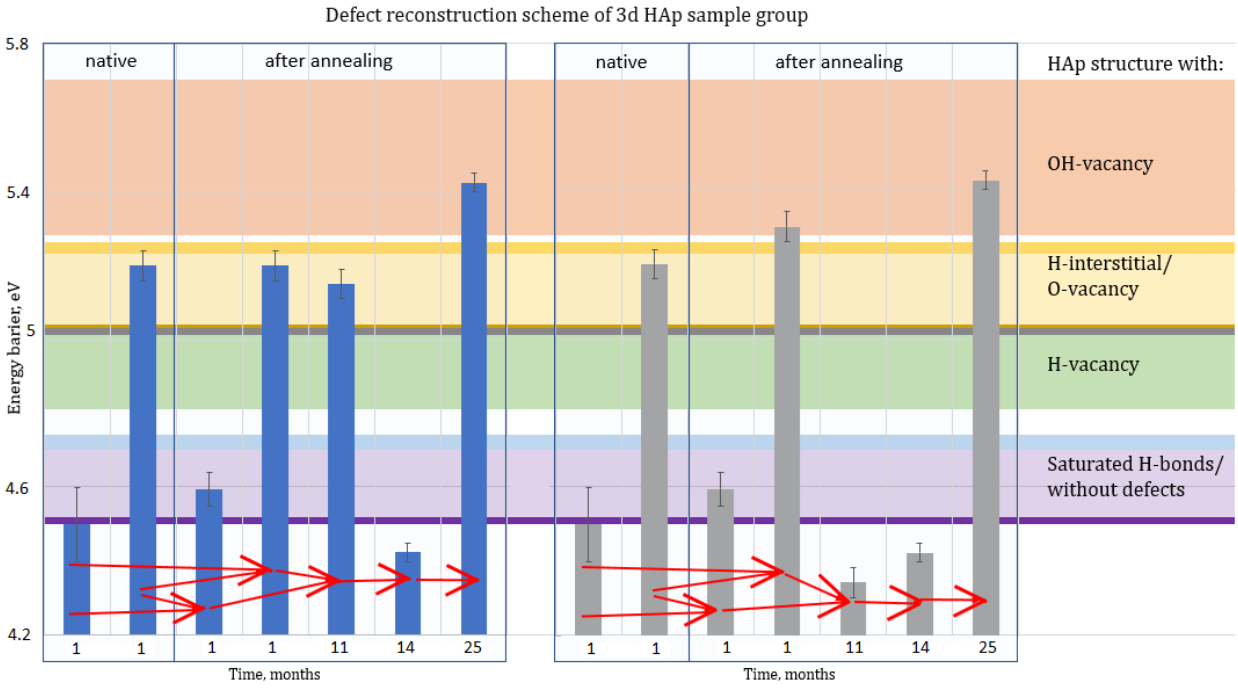

Fig. 3.8. Schemes of defect reconstructions in samples of the Group 3.

After 11 and 14 months, the measured EWF values of the samples of Subgroup 1 began to correspond to the calculated EWF value of HAp without defects in the structure. After 25 months, the measured EWF values of the samples of Subgroup 1 began to correspond to the calculated EWF value of HAp with OH-vacancy.

After 11 months, the measured EWF values of the samples of Subgroup 2 began to correspond to the calculated EWF value of HAp with O-vacancy. After 14 months, the measured EWF values of the samples of Subgroup 2 began to correspond to the calculated EWF value of HAp without defects in the structure. After 25 months, the measured EWF

values of the samples of Subgroup 2 began to correspond to the calculated EWF value of HAp with OH-vacancy.

After annealing, two E_{Ai} from the samples of Group 4 (whose initial values of E_{Ai} correspond to the calculated EWF values of HAp with saturated hydrogen bonds and OH-vacancy in the structure) were registered (Fig. 3.9): the first one with an average value of 4.62 eV, which corresponds to the calculated value of EWF = 4.63 eV of HAp with saturated hydrogen bonds, and the second – 5 eV, which corresponds to the calculated value of EWF = 4.92 eV of HAp with H-vacancy.

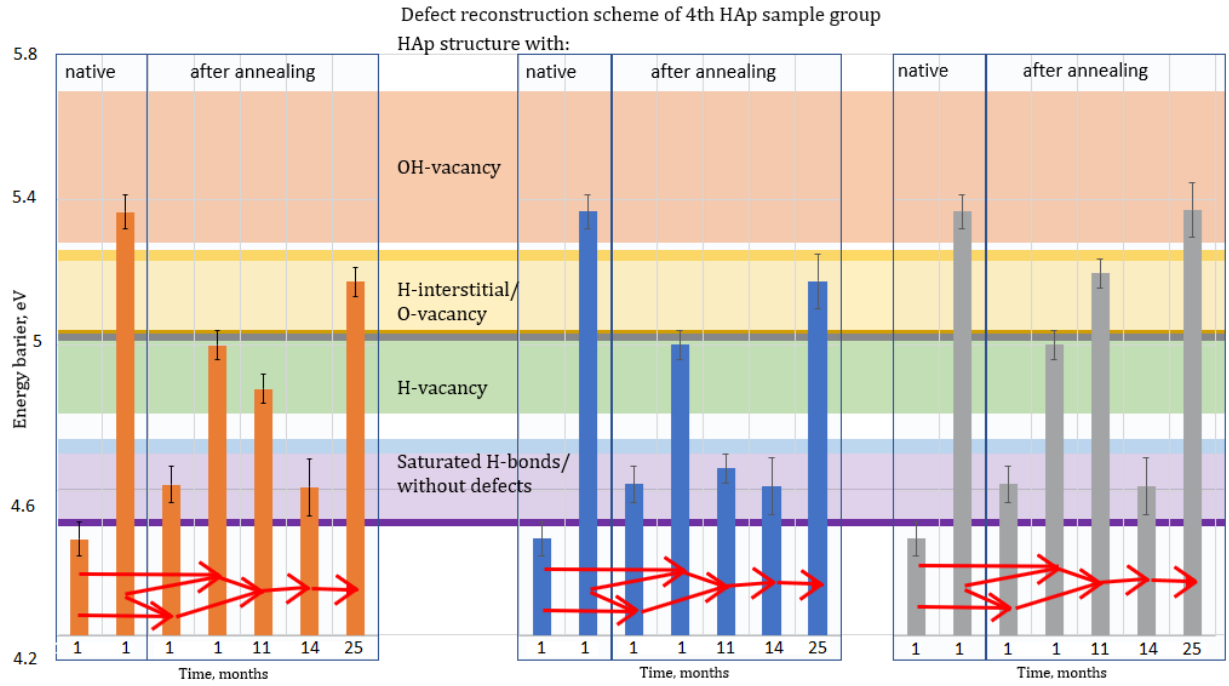

Fig. 3.9. Schemes of defect reconstructions in samples of the Group 4.

After 11 months, samples of the fourth group were sorted into 3 subgroups according to EWF values:

- Subgroup 1 (on the left in Fig. 3.9) – samples with an average value of EWF = 4.88 eV, which corresponds to the calculated value of EWF = 4.92 eV of HAp with H-vacancy;
- Subgroup 2 (in the centre of Fig. 3.9) – samples with an average value of EWF = 4.66 eV, which corresponds to the calculated values of EWF of HAp with saturated hydrogen bonds or without structural defects;
- Subgroup 3 – samples with an average value of EWF = 5.2 eV, which corresponds to the calculated value of EWF = 5.15 eV of HAp with O-vacancy.

After 14 months, the measured EWF values of the samples of all three subgroups began to correspond to the calculated EWF values of HAp with saturated hydrogen bonds or without structural defects.

After 25 months, the measured EWF values of the samples of Subgroups 1 and 2 began to correspond to the calculated EWF value of HAp with O-vacancy.

After 25 months, the measured EWF values of the samples of Subgroup 3 began to correspond to the calculated EWF value of HAp with OH-vacancy.

After annealing two E_{Ai} from the samples of Group 5 (whose initial E_{Ai} values correspond to the calculated EWF values of HAp with O-vacancy and H-vacancy in the structure) were registered (Fig. 3.10): the first one with an average value of 4.85 eV, which corresponds to the calculated EWF value of HAp with saturated hydrogen bonds, and the second – 5.08 eV, which corresponds to the calculated EWF value of HAp with H-vacancy.

After 11 months, the measured EWF values of the samples of Group 5 began to correspond to the calculated EWF value of HAp with OH-vacancy.

After 14 months, the measured EWF values of the samples of Group 5 began to correspond to the calculated EWF values of HAp with saturated hydrogen bonds or without structural defects.

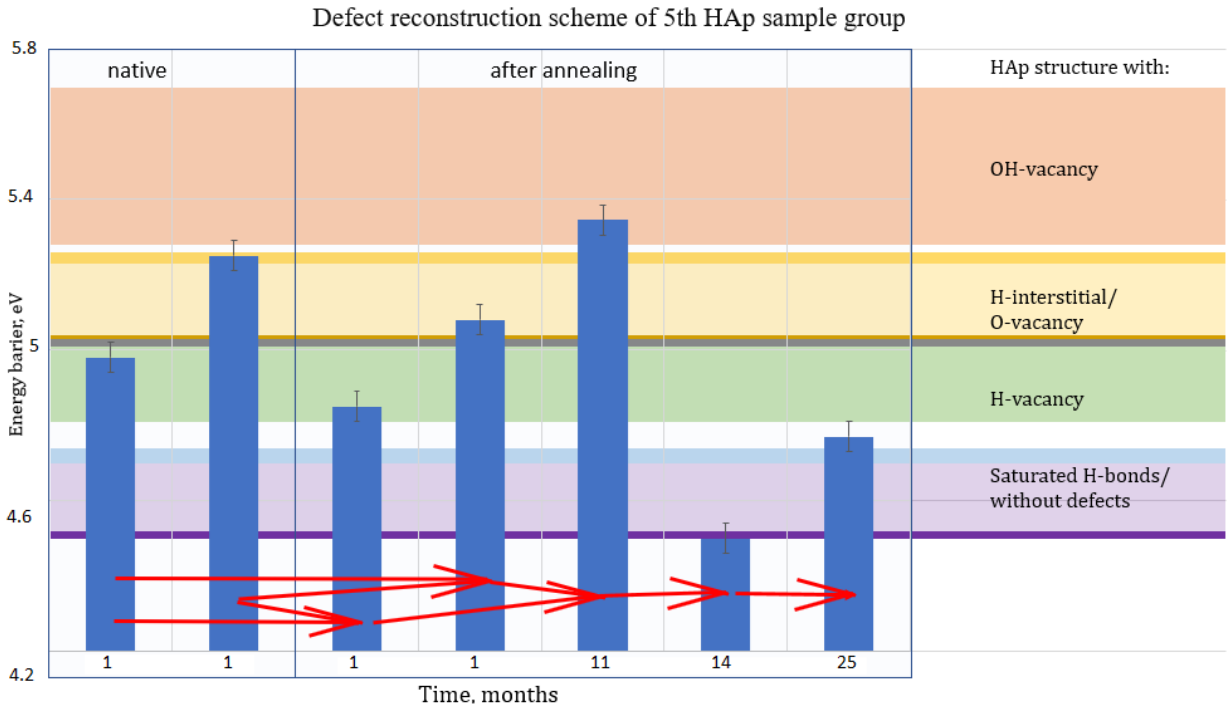

Fig. 3.10. Scheme of defect reconstruction in samples of Group 5.

After annealing, two E_{Ai} from the samples of Group 6 (whose initial EWF values correspond to calculated EWF values of HAp with O-vacancy or H-interstitial) were registered (Fig. 3.11): the first one with an average value of 4.7 eV, which corresponds to the calculated EWF value of HAp with saturated hydrogen bonds, and the second – 5.15 eV, which corresponds to the calculated EWF value of HAp with O-vacancy.

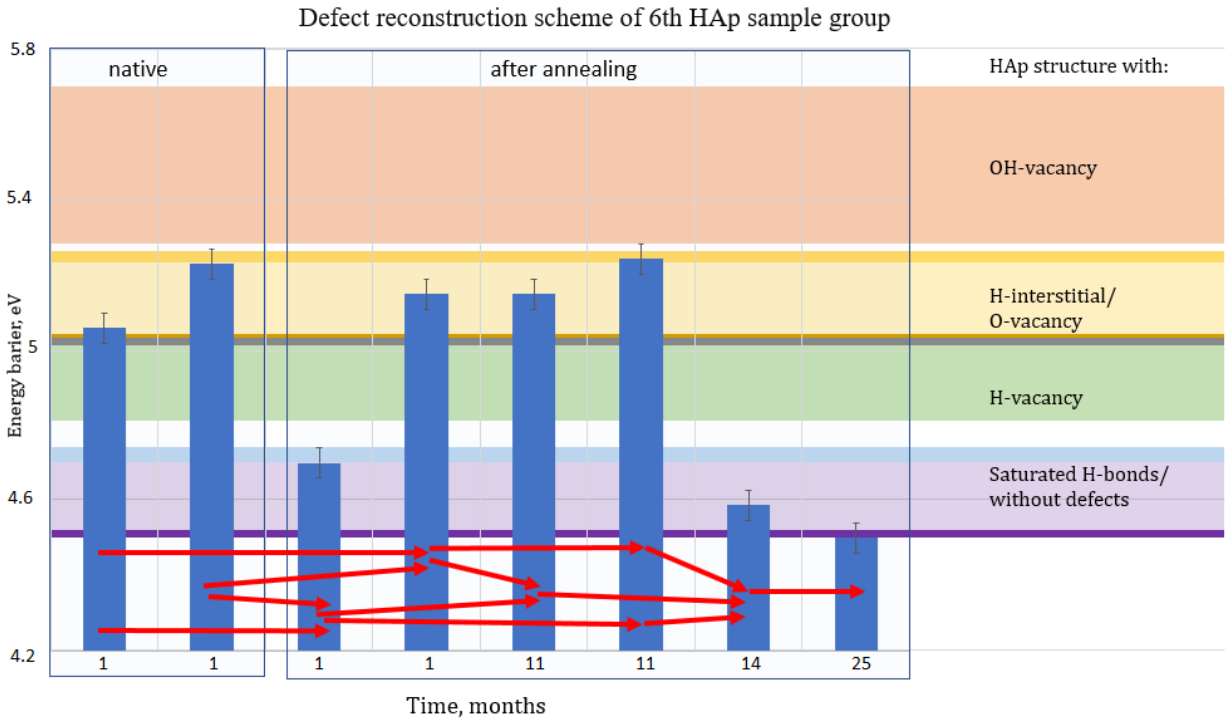

Fig. 3.11. Scheme of defect reconstruction in samples of Group 6.

After 11 months, the measured EWF values of the samples of Group 6 began to correspond to the calculated EWF value of HAp with O-vacancy.

After 14 and 25 months, the measured EWF values of the samples of Group 6 began to correspond to the calculated EWF values of HAp with saturated hydrogen bonds or without defects in the structure.

Figure 3.12 shows various annealing-induced defect transformations over time. OH-, H-, O- vacancies, H-interstitials and saturated hydrogen bonds exist in HAp samples initially. After annealing, there are no H-interstitials in the structure of HAp samples, but there are O-, H-, OH-vacancies that remain for at least 11 months. After 14 months, these defects disappear, but then structural imperfections such as H-interstitials, O-, H-, OH-vacancies can spontaneously appear.

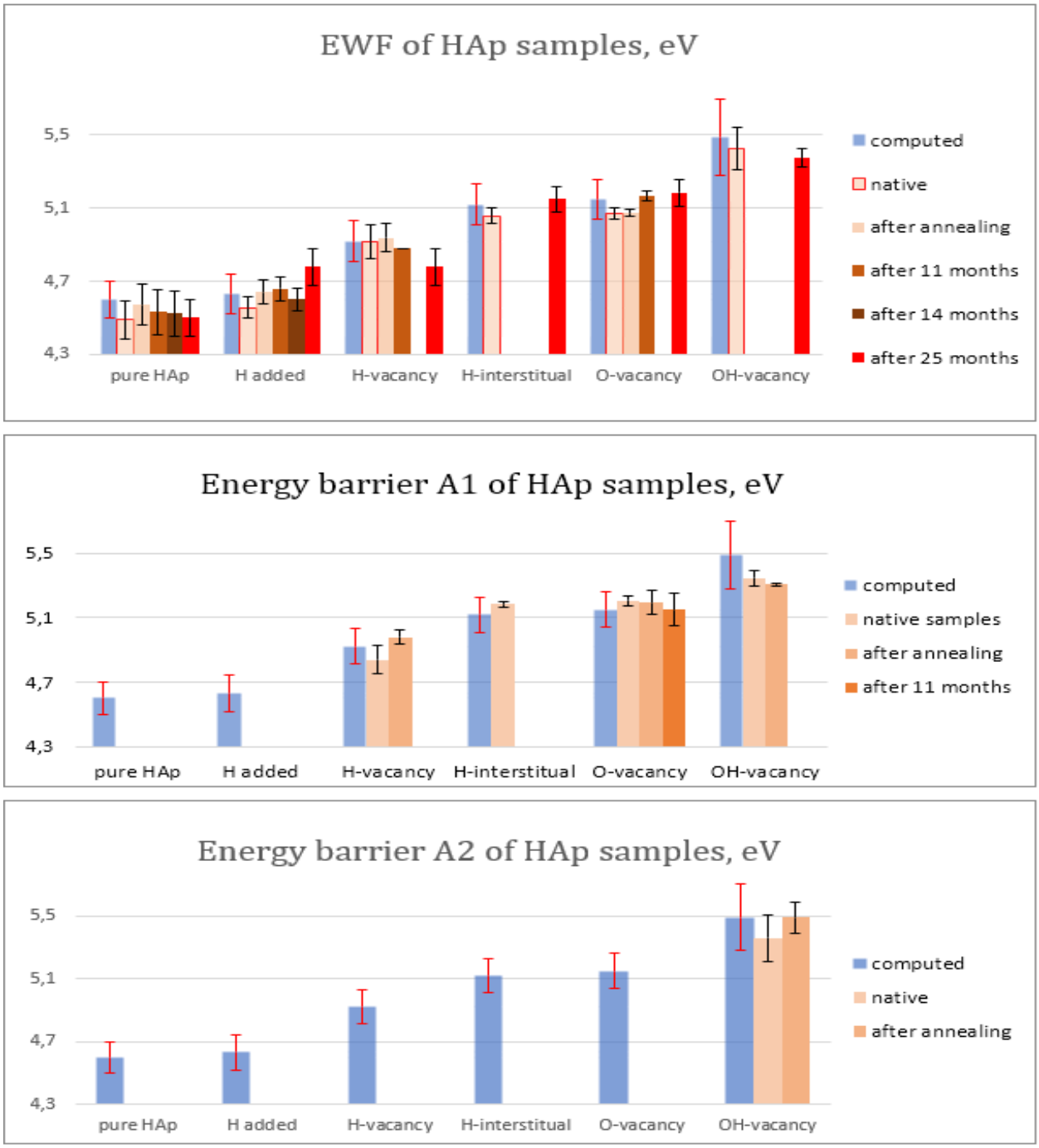

Fig. 3.12. Schemes of the transformation of HAp structural defects after annealing (detailed description in Subsection 3.7.2).

3.7.3. Influence of annealing and gamma-ray irradiation on HAp

After annealing, the samples (whose initial EWF values correspond to the calculated EWF of HAp with OH-vacancy) were sorted into two subgroups according to the E_{Ai} values in the same way as the initial samples were grouped (Subsection 3.7.2, Fig. 3.14):

- Subgroup 1 (on the left in Fig. 3.14) – samples with two E_{Ai}: the first one with an average value of 5.6 eV, which corresponds to the calculated value of EWF = 5.49 eV of HAp with OH-vacancy, and the second – 4.93 eV, which corresponds to the calculated value of EWF = 4.92 eV of HAp with H-vacancy;

- Subgroup 2 (on the right in Fig. 3.14) – HAp samples with two E_{Ai}: the first one with an average value of 5.12 eV, which corresponds to the calculated value of EWF = 5.15 eV of HAp with O- vacancy and the second – 4.93 eV, which corresponds to the calculated value of EWF = 4.92 eV of HAp with H-vacancy.

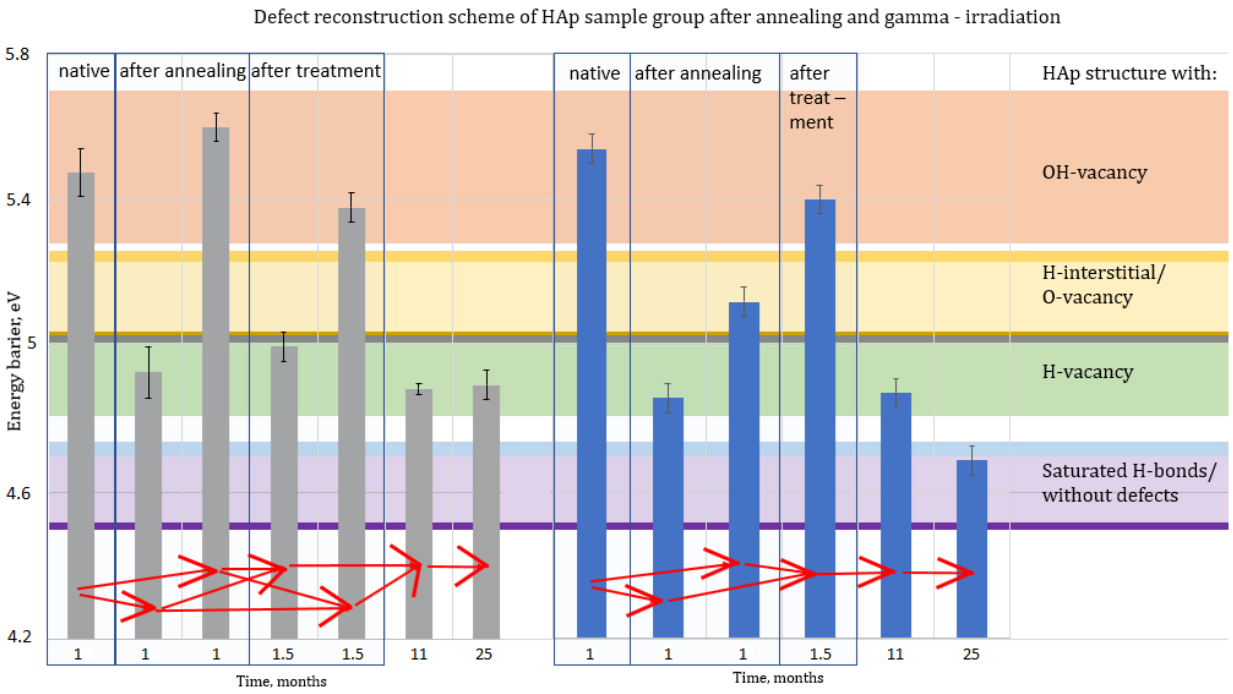

Fig. 3.13. Schemes of defect reconstructions in HAp after annealing and gamma-ray irradiation.

After gamma-ray irradiation, two E_{Ai} from the samples of Subgroup 1 were registered: the first one with an average value of 5.38 eV, which corresponds to the calculated value of EWF = 5.49 of HAp with OH-vacancy, and the second – 5 eV, which corresponds to the calculated value of EWF = 4.92 eV of HAp with H-vacancy.

After gamma-ray irradiation, the measured EWF value of samples of Subgroup 2 was 5.4 eV, which corresponds to the calculated value of EWF = 5.49 eV of HAp with OH-vacancy.

After 11 months, the measured EWF values of the samples of both subgroups began to correspond to the calculated EWF value of HAp with H-vacancy. After 25 months, the measured EWF values of the samples of Subgroup 1 began to correspond to the calculated EWF value of HAp with H-vacancy, and the measured EWF values of the samples of Subgroup 2 began to correspond to the calculated EWF values of HAp with saturated hydrogen bonds or without defects in the structure.

Based on these experimental data, the following conclusions are drawn:

1) initially HAp samples of this group had OH-vacancies in the structure;
2) changes in the structure of HAp samples after annealing and gamma-ray irradiation happened due to the following competing processes: annealing leads to an increase in the number of OH-vacancies, while gamma-ray irradiation forms dissociated H^+ and OH^- ions in HAp, which can penetrate OH-channels. This process leads to an increase in the number of occupied OH-vacancies that compensates the results of annealing;

3) O-vacancies in HAp structure form under influence of gamma-ray irradiation, because the value of EWF, which corresponds to the calculated EWF value of HAp with this type of defect, was registered in this experiment.

3.7.4. Influence of annealing and hydrogenation on HAp

After annealing, the samples (the initial EWF values of which correspond to the calculated EWF values of HAp with H-vacancy and HAp with O-vacancy or H-interstitial) were sorted into two subgroups according to the measured EWF values in the same way as the initial samples were grouped (Fig. 3.14):

- Subgroup 1 (on the left in Fig. 3.14) – HAp samples with an average value of EWF = 4.95 eV, which corresponds to the calculated value of EWF = 4.92 eV of HAp with H-vacancy;
- Subgroup 2 – samples with an average value of EWF = 4.62 eV, which corresponds to the calculated values of EWF = 4.63 eV of HAp with saturated hydrogen bonds or without defects in the structure.

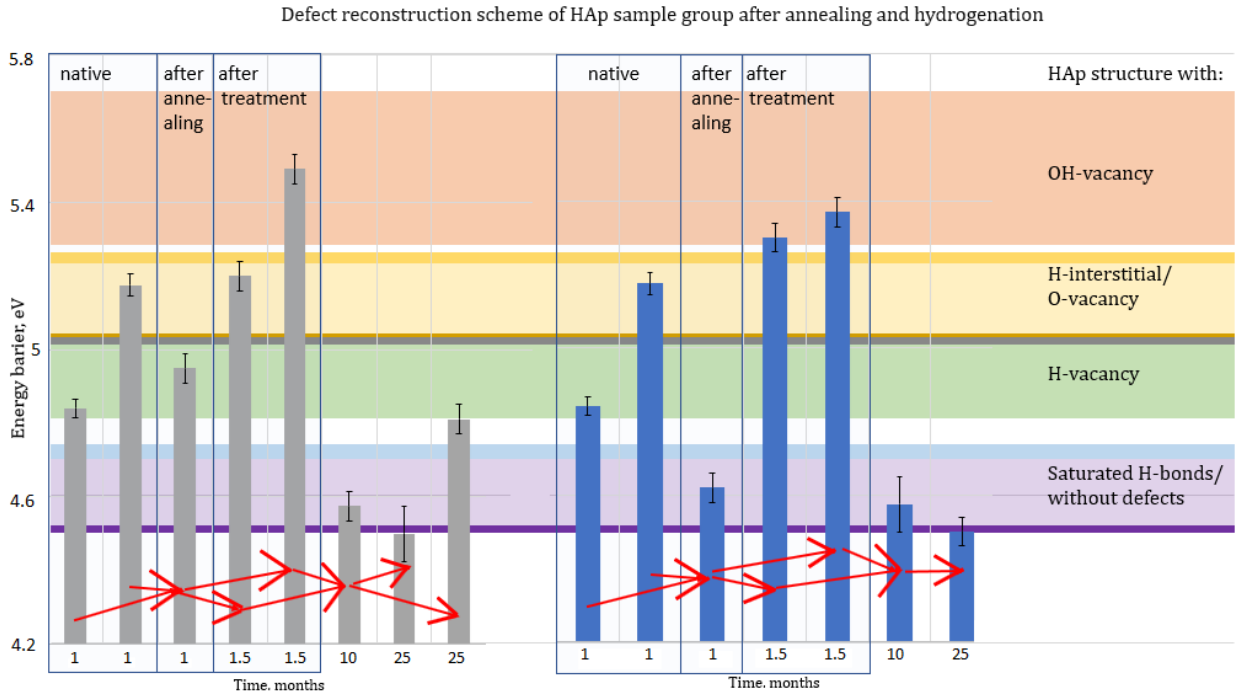

Fig. 3.14. Schemes of defect reconstructions in HAp after annealing and hydrogenation.

After hydrogenation, two E_{Ai} from the samples of Subgroup 1 were registered: the first one with an average value of 5.2 eV, which corresponds to the calculated EWF values of HAp with O-vacancy or H-interstitial, and the second – 5.49 eV, which corresponds to the calculated value of EWF = 5.49 eV of HAp with OH-vacancy.

After hydrogenation, the values of two registered E_{Ai} from the samples of Subgroup 2 (5.30 eV and 5.37 eV) corresponded to the calculated EWF value of HAp with OH-vacancy. The PL spectra of this subgroup's samples were measured after hydrogenation.

After 10 months, the measured EWF values of the samples of both subgroups began to correspond to the calculated EWF values of HAp with saturated hydrogen bonds or without structural defects. This means that this combination of treatments produces OH-vacancies, but after some time the OH-groups have formed and filled these vacancies.

After 25 months, two E_{Ai} from the samples of Subgroup 1 were registered: the first one corresponds to the calculated EWF value of HAp with H-vacancy, and the second one corresponds to the calculated EWF value of HAp with saturated hydrogen bonds.

After 25 months, the measured EWF values of the samples of Subgroup 2 began to correspond to the calculated EWF values of HAp with saturated hydrogen bonds or without defects in the structure.

Based on these experimental data, the following conclusion is made: hydrogenation induces H-interstitials, but they are unstable and disappear within 11 months.

3.7.5. Influence of annealing and microwave irradiation on HAp

Before annealing, the samples were sorted into two groups according to the E_{Ai} values in the same way as the initial samples were grouped (Subsection 3.7.2, Fig. 3.15):

- Group 1 (on the left in Fig. 3.16) – samples with three E_{Ai}: the first one with an average value of 4.5 eV, which corresponds to the calculated EWF value of HAp with saturated hydrogen bonds, the second – 5 eV, which corresponds to the calculated value of EWF = 4.92 eV of HAp with H-vacancy, and the third – 5.18 eV, which corresponds to the calculated EWF values of HAp vacancy with O-vacancy or H-interstitial;
- Group 2 – samples with two E_{Ai}: the first one with an average value of 5.17 eV, which corresponds to the calculated EWF values of HAp with O-vacancy or H-interstitial; and the second, 5.33 eV, which corresponds to the calculated EWF value of HAp with OH- vacancy.

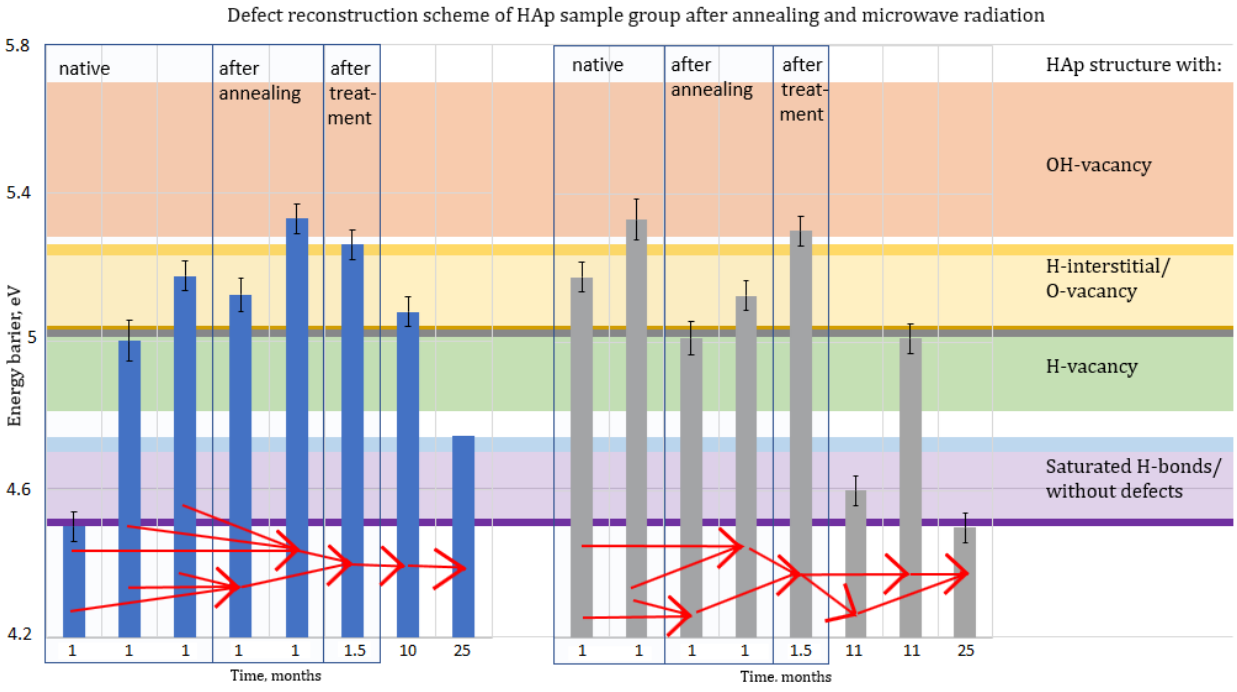

Fig. 3.15. Schemes of defect reconstructions in HAp after annealing and microwave irradiation.

After annealing, two E_{Ai} from the samples of Group 1 were registered: the first one with an average value of 5.12 eV, which corresponds to the calculated EWF value of HAp with O-vacancy, and the second – 5.33 eV, which corresponds to the calculated EWF value of HAp with OH-vacancy.

After annealing, two E_{Ai} from the samples of Group 2 were registered: the first one with an average value of 5.01 eV, which corresponds to the calculated EWF value of HAp with H-vacancy, and the second – 5.13 eV, which corresponds to the calculated EWF value of HAp with O-vacancy.

After microwave irradiation, the measured EWF values of the samples of Group 1 began to correspond to the calculated EWF values of HAp with O-vacancy or H-interstitial.

After microwave irradiation, the measured EWF values of the samples of Group 2 began to correspond to the calculated EWF value of HAp with OH-vacancy.

After 10 months, the measured EWF values of the samples of Group 1 still corresponded to the calculated EWF values of HAp with O-vacancy or H-interstitial.

After 11 months, two E_{Ai} from the samples of Group 2 were registered: the first one with an average value of 4.6 eV, which corresponds to the calculated EWF values of HAp with saturated hydrogen bonds or without defects in the structure, and the second – 5.01 eV, which corresponds to the calculated EWF value of HAp with H-vacancy.

After 25 months, the measured EWF values of the samples of both groups began to correspond to the calculated EWF values of HAp with saturated hydrogen bonds or without defects in the structure.

Based on these experimental data, the following conclusion is drawn: microwave irradiation induces H-interstitials that stay inside the HAp structure for 11 months.

3.7.6. Influence of annealing, hydrogenation, and microwave irradiation on HAp

Before annealing, the samples were sorted into two groups according to the E_{Ai} values in the same way as the initial samples were grouped (Section 3.7.2, Fig. 3.17):

- Group 1 (on the left in Fig. 3.17) – samples with two E_{Ai}: the first one with an average value of 5.01 eV, which corresponds to the calculated EWF value of HAp with H-vacancy, and the second – 5.4 eV, which corresponds to the calculated value of EWF = 5.49 eV of HAp with OH-vacancy;
- Group 2 – samples with two E_{Ai}: the first one with an average value of 5.04 eV, which corresponds to the calculated EWF value of HAp with H-vacancy, and the second – 5.2 eV, which corresponds to the calculated EWF values of HAp with O-vacancy or H-interstitial.

After annealing, two E_{Ai} from the samples of Group 1 were registered: the first one with an average value of 5.07 eV, which corresponds to the calculated EWF value of HAp with O-vacancy, and the second – 5.31 eV, which corresponds to the calculated EWF value of HAp with OH-vacancy.

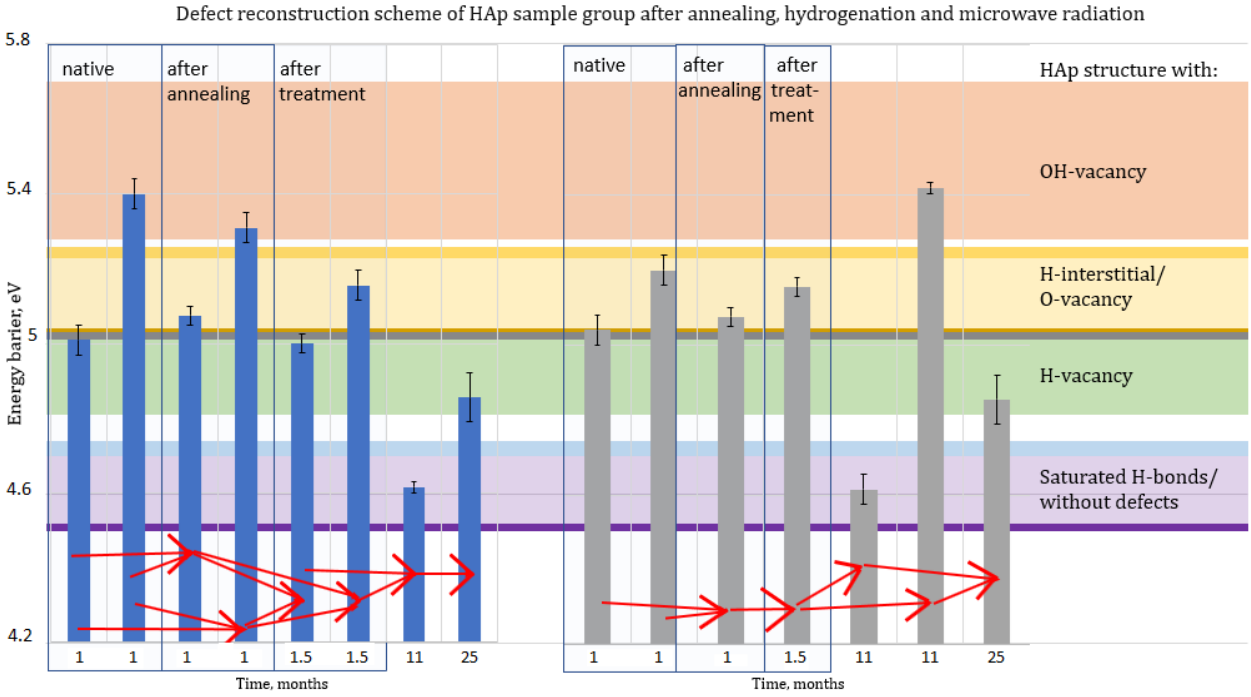

Fig. 3.16. Schemes of defect reconstructions in HAp after annealing, hydrogenation, and microwave irradiation.

After annealing, the measured EWF values of the samples of Group 2 began to correspond to the calculated EWF value of HAp with O-vacancy.

After hydrogenation and microwave irradiation, two E_{Ai} from the samples of Group 1 were registered: the first one with an average value of 5.0 eV, which corresponds to the calculated EWF value of HAp with H-vacancy, and the second – 5.16 eV, which corresponds to the calculated EWF values of HAp with O-vacancy or H-interstitials.

After hydrogenation and microwave irradiation, the measured EWF values of the samples of Group 2 began to correspond to the calculated values of EWF of HAp with O-vacancy or H-interstitial.

After 11 months, the measured EWF values of the samples of Group 1 began to correspond to the calculated EWF values of HAp with saturated hydrogen bonds or without defects in the structure. After 11 months, two E_{Ai} from the samples of Group 2 were registered: the first one with an average value of 4.62 eV, which corresponds to the calculated EWF value of HAp with saturated hydrogen bonds, and the second – 5.42 eV, which corresponds to the calculated EWF value of HAp with OH-vacancy.

The results of this experiment show that unlike the defects induced by microwave irradiation, which are stable and stay inside HAp structure for 11 months, the defects formed by hydrogenation are unstable (Fig. 3.16). It is also likely that microwave irradiation inserts the H-interstitials deeper into the structure of the HAp sample along OH-channels, and interactions between the H-interstitials and O-vacancies arise, that lead to an increase of quantity of OH-vacancies over time. After 25 months OH-vacancies were not detected in the HAp samples.

After 25 months, the measured EWF values of the samples of both groups corresponded to the calculated EWF value of HAp with H-vacancy. It means that the inserted H atoms did not have enough energy to form stable bonds for more than 2 years.

Based on these experimental data, the following conclusion can be drawn: the use of hydrogenation of samples to insert hydrogen atoms into the HAp structure and following processing them by microwave irradiation to penetrate these H atoms deeper into the HAp structure is justified.

3.7.7. Analysis of the PL spectra

The PL spectra were registered for samples processed by all technologies (annealing, irradiation with microwave radiation and gamma radiation, hydrogenation) (Figs. 3.17 and 3.18).

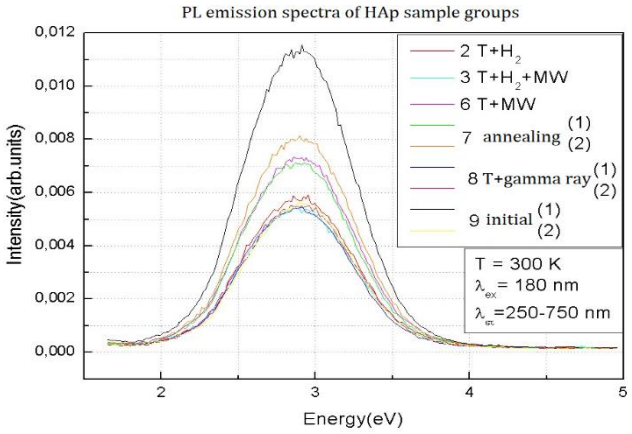

Fig. 3.17. PL emission spectra.

The registered PL maximum (2.95 eV) corresponds to local levels with an energy of 2.95 eV. The average width of the peaks at half maximum is approximately (1.0 ± 0.1) eV in the range from ~2.4 eV to ~3.4 eV.

Since the band gap width of a HAp without defects is 4.6 eV (Part 2), in the case of a HAp without defects, PL cannot be fixed. Accordingly, in our samples there are defects that give additional levels (or a narrow zone) inside the band gap. According to theoretical calculations (Part 2), the OH-vacancy in the unit cell induces energy levels inside the band gap: E_c = (2.5–1.7) eV and presence of OH-vacancy increases the width of the band gap (till 5.49 eV) (Table 2.2, [28, 33]) This shift leads to an increase in the EWF value by 0.89 eV. This change is registered experimentally (Subsections 3.7.2–3.7.4 and 3.7.6).

According to theoretical calculations (Part 2, Table 2.2), the H-interstitial in the unit cell induces energy levels inside the band gap: E_c = (3.9–3.4) eV and the presence of H-interstitial increases the band gap width (till 5.12 eV) (Table 2.2, [28, 33, 37, 44]). This shift leads to an increase in the EWF value by 0.52 eV. This change is registered experimentally (Subsections 3.7.3, 3.7.4 and 3.7.6).

In both cases, the levels inside the band gap are half filled with electrons and can serve as recombination centres (Part 2).

Thus, the combined levels induced by these defects form an energy band in the middle of band gap, which corresponds to the PL energy interval (2.95 eV ± 0.5 eV) registered in the experiment.

In addition, energy levels can be induced by the formation of bonds between hydrogen and oxygen from the PO_4 group. As obtained in this work (Part 2), in this case, the transfer energy from the local level E_{i1} to the bottom of the conductive band is ΔE_{i1} = (2.92 ± 0.05) eV. This value corresponds to the experimentally obtained value of the PL peak (2.95 eV). Therefore, the corresponding energy centre can also play the role of a recombination centre and PL.

The PL excitation spectra in the energy range from 3.5 eV to 18 eV, registered on the PL line (2.95 eV), after all types of sample processing are shown in Fig. 3.18. This figure (left) shows the full spectrum obtained, whereas parts of the spectra in the range from 7.5 eV to 18 eV are presented in the figure on the right.

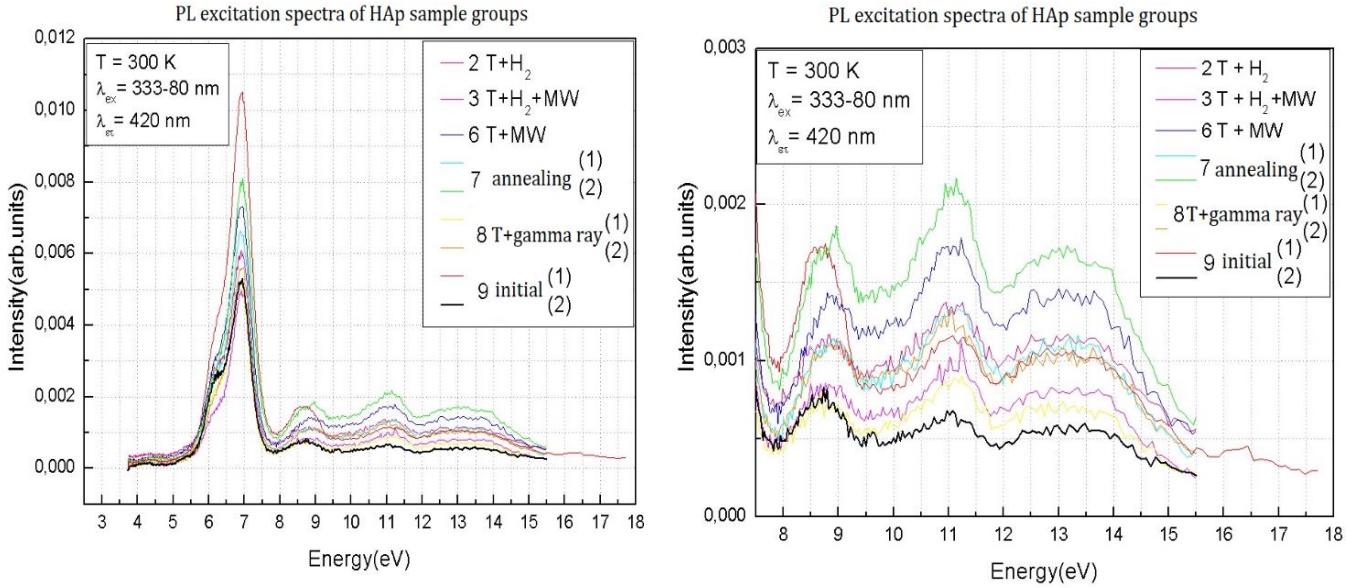

Fig. 3.18. PL excitation spectra at λ= 420 nm: left – in the range of 3.5–18 eV; right – in the range of 7.5–18 eV.

From calculations of HAp DOS (Part 2, [24, 31, 33]), it is known that there are DOS peaks (called A, B, C, D) in the valence band of a HAp without structural imperfections. These peaks are produced by combinations of electron orbitals of HAp atoms:

1) peak A − components of the P 3s and O 2p orbitals;
2) peak B − components of orbitals P 3p and O 2p;
3) peaks C and D are the components of the O 2p orbitals with Ca 4s and 3d.

In the range of deep levels (from around −21 eV till −18 eV), peaks are produced by mixing the components of the O 2s orbitals with P 3s and P 3p.

The components of the Ca 3d orbitals correspond to the conductive band (Part 2, [28, 33]).

The comparison of the ionization potentials (IP) values of the corresponding HAp atoms with the energies of the registered peaks (Fig. 3.19) leads to the conclusions that:

1) the first IP Ca ~6 eV corresponds to D peak (5.5–7.5 eV);

2) the first IP of the phosphorus atom (which is close to 10.5 eV − value of IP for an isolated atom) and IP of the calcium atom (whose value for the isolated atom is ~11.87 eV) correspond to peak C (8.0–9.5 eV) and peak B (10–12 eV);
3) the first IP of the oxygen atom (whose value is ~13.6 eV) corresponds to peak A (12–14 eV).

Thus, the registered energy peaks (Fig 3.18) correspond to the energies of excitation of electrons from the valence band to the conductive band of the HAp.

To obtain PL peaks corresponding to different electron excitation energies, it is necessary that the electrons are captured by the recombination centre inside the band gap. According to calculations (Part 2) there are no centres with energy levels inside the band gap in a HAp without defects. As it was established above, there is a PL emission peak with an energy level of 2.95 eV, located approximately in the middle of the band gap in the HAp samples used in this work. This peak is induced by defects in the structure. It is possible to produce defects in the HAp structure using all the above-mentioned impacts (Part 3). In particular, hydrogenation can affect hydrogen bonds, as well as bonds of atoms having high affinity for hydrogen (oxygen). As a result, complexes of various defects (vacancy of various types (H-, O-, or OH-) and inserted H-interstitials) can form.

Thus, peaks A, B, C, D and deep levels were firstly registered experimentally in this work.

Scheme of electron excitation by synchrotron irradiation and the PL process are shown in Fig. 3.19. As a result of irradiation with synchrotron radiation, the following processes occur (Fig. 3.19):

1) electron transfer from the valence band from peaks A, B, C, D and from deep levels to the conductive band;
2) thermalization of excited electrons to the bottom of the conductive band;
3) the electron transition and their capture on the local energy levels inside band gap, induced by OH-vacancies, H-interstitials and H atoms saturating unsaturated hydrogen bonds;
4) the recombination of electrons that have fallen to local levels of the band gap with the “holes” mentioned above at local energy levels inside band gap;
5) emission of luminescence photons with an average energy $E_i \approx (2.95 \pm 0.50)$ eV (as shown schematically by arrows in Fig. 3.19).

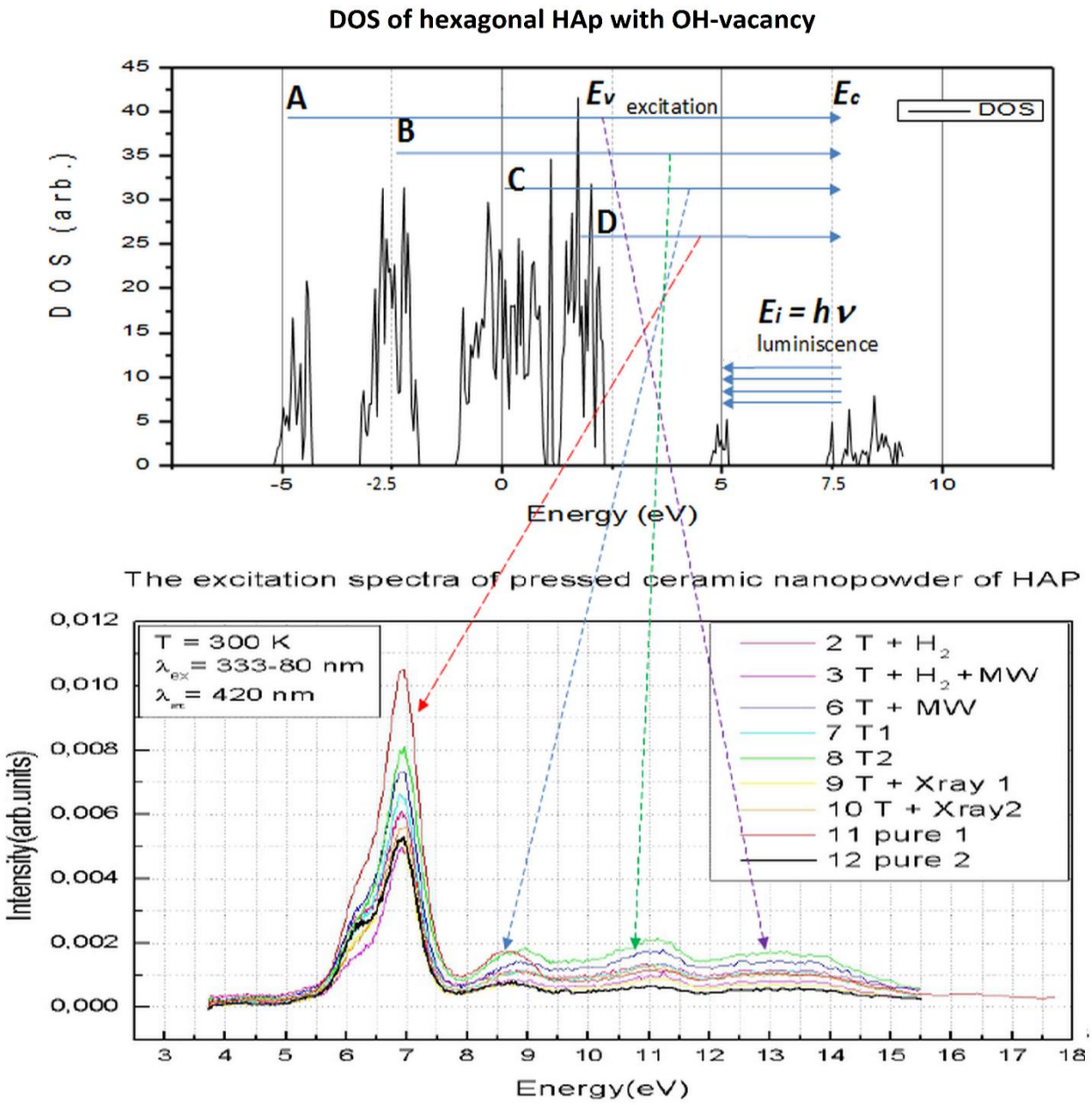

Fig. 3.19. Scheme of electron excitation by synchrotron irradiation and the PL process.

CONCLUSION

The Thesis results explain the physical mechanism of HAp surface electrical potential changes, depending on presence of structural imperfections.

The following main results were achieved in the Thesis.

1. Models of HAp crystal cells and clusters were constructed using HyperChem software tool, including molecular mechanics (BIO+CHARMM) and semi-empirical quantum methods (PM3). Based on these models, the values of following parameters were calculated for HAp clusters and for HAp crystal cells with various structural defects: the total energies of the structures, the energies of their electron subsystems in the energy band diagram, the width of band gap and electron work function, dipole moments and polarization. The influence of hydrogen atoms on the above parameters was estimated. It was shown that the width of band gap, the value of EWF, the value and orientation of the dipole moment, the polarization of HAp crystal unit cells and clusters depend on the quantity and location of hydrogens in the structure, the size and shape of the HAp cluster. The polarization value (P) varies in the range from 0.01 C/m to 0.15 C/m^2 depending on the magnitude of the applied electric field and temperature. In the absence of an external electric field, a spontaneous polarization $P \approx 0.01$ C/m^2 occurs in the hydroxyapatite, which means that HAp has ferroelectric properties.
2. Using the methods of the density functional theory in the local density approximation (LDA DFT), the HAp structure without defects and the structures of HAp crystal unit cells with defects (O-, H-, OH vacancies, H-interstitial, or two hydrogen atoms filling unsaturated hydrogen bonds) were calculated. Based on these calculations, the influence of the above structural imperfections on the changes of HAp surface charge, HAp electric potential, EWF and the width of band gap was estimated:
   a) OH-vacancies:
      - increase the width of band gap (E_g) by ~0.86 eV (from $E_g \approx 4.6$ eV for hexagonal HAp without defects in structure to $E_g \approx 5.49$ eV);
      - produce local energy levels inside the band gap. These levels are half occupied by electrons, and located in the range of $E_i \approx E_v$ + (3.11–3.82) eV with peaks at 3.40 eV, 3.53 eV and 3.66 eV. These levels are the recombination centres of electrons and “holes”;
   b) O-vacancies of the OH-group:
      - produce local energy levels inside the band gap, which are located close to the top of the valence band ($E_i = E_v + 0.1$ eV);
      - increase the width of band gap from 4.6 eV (for hexagonal HAp without defects in structure) to 5.15 eV;
   c) H-vacancies of the OH-group:
      - produce local energy levels inside the band gap, which are located close to the top of the valence band ($E_i = E_v + 0.1$ eV);

- increase the width of band gap from 4.6 eV (for hexagonal HAp without defects in structure) to 4.92 eV;

d) H-interstitials change the width of band gap from 4.6 eV (for hexagonal HAp without defects in structure) to 5.12 eV and produce three local energy levels inside the band gap ($E_i = E_v$ + 1.20 eV, 1.45 eV and 1.75 eV). These levels are half occupied by electrons. These levels are the recombination centres of electrons and "holes";

e) two hydrogen atoms filling unsaturated hydrogen bonds change the width of band gap from 4.6 eV (for a hexagonal HAp without defects in structure) to 4.63 eV and produce local energy levels inside the band gap ($E_{i1} \approx E_c$ – 2.92 eV and $E_{i2} \approx E_c$ – 3.74 eV). These levels are filled with electrons.

3. Results of experiments carried out for investigating the influence of the different treatments listed below on HAp surface charge changes established the following:

a) annealing at 542–546 °C for 30 minutes destroys and rearranges hydrogen and some covalent bonds (from OH, PO_4-groups) in the following ways:

- the release of hydrogen from the OH-group;
- oxygen release from OH or PO_4-groups;
- the release of the OH-group from the HAp OH-channel structure;
- capture of hydrogen atoms on unsaturated hydrogen bonds.

Reconstruction of the above-mentioned bonds obtained due to annealing depends on the presence of different types of defects in the structure of the initial HAp sample.

b) after gamma-ray irradiation, the values of the measured energy barriers for the electron exit from HAp (5.40 eV ± 0.04 eV, 5.00 eV ± 0.04 eV) correlate with the calculated values of EWF from HAp with OH-vacancy (5.49 eV ± 0.21 eV) and H-vacancy (4.92 eV ± 0.11 eV). This means that during gamma-rays irradiation, OH-vacancies and H-vacancies are formed in the structure of the investigated samples.

c) after microwave irradiation (800 W), the values of the measured energy barriers for the electron exit from HAp (5.30 eV ± 0.04 eV, 5.26 eV ± 0.04 eV) correlate with the calculated values of EWF from HAp with OH-vacancy (5.49 eV ± 0.21 eV) and O-vacancy (5.15 eV ± 0.11 eV) or H-interstitial (5.12 eV ± 0.11 eV). This means that during microwave irradiation, OH-vacancies and O-vacancies or H-interstitials are formed in the structure of the investigated samples.

d) after hydrogenation, the values of the measured energy barriers for the electron exit from HAp (5.39 eV ± 0.08 eV, 5.20 eV ± 0.04 eV) correlate with the calculated values of EWF from HAp with OH-vacancy (5.49 eV ± 0.21 eV) and O-vacancy (5.15 eV ± 0.11 eV) or H-interstitial (5.12 eV ± 0.11 eV). This means that during hydrogenation, OH-vacancies and O-vacancies or H-interstitials are formed in the structure of the investigated samples. Hydrogen atoms penetrate deeper into the HAp structure through OH-channels.

All calculated data of the investigated structures and HAp properties are in line with experimental data with an error of ±2.2 %.

4. A comparison of the calculated electron density of states (DOS) of HAp structures with various types of defects with the results of measurements of energy levels in the HAp band structure proved the presence of local energy levels inside the band gap of investigated HAp samples corresponding to the presence of various structural imperfections. These levels serve as electron capture centres as well as electron and "hole" recombination centres. A PL centre with an energy of 2.95 eV and a half-width of ~1 eV was established experimentally, which is associated with the presence of OH-vacancies, H-interstitials, and hydrogen atoms filling unsaturated hydrogen bonds.

The results can be used for technological management of structural defects for functionalization of the HAp surface by changing electric charge density of its surface for biomedical applications.

Recommendations

The obtained results allow suggesting a recommendation to engineer the surface potential of HAp samples to improve the cells' adhesion – to anneal the sample at temperature 542–546 °C for 30 minutes, and afterwards to hydrogenate for 6 hours at settings (60 ± 2) atm under $t = 23$ °C or/and apply microwave irradiation (power 800 W) for 6.5 minutes for deeper penetration of protons in the samples.

LIST OF LITERATURE

1. Becker E. L., Landau S. I., Manuila A. International dictionary of medicine and biology. New York: Wiley, 1986. 3200 p.
2. Rather B. D. et al. Biomaterial Science. London: Academic Press, 1996. 879 p.
3. Best S. M., Porter A. E., Thian E. S., Huang J. Bioceramics: Past, present and for the future. Journal of the European Ceramic Society. 2008. Vol. 28. pp. 1319–1327. DOI: 10.1016/j.jeurceramsoc.2007.12.001.
4. Epple M., Ganesan K., Heumann R., Klesing J., Kovtun A., Neumann S., Sokolova V. Application of calcium phosphate nanoparticles in biomedicine. Journal of Materials Chemistry. 2010. Vol. 20. pp. 18–23.
5. Dorozhkin S. V. Nanosized and nanocrystalline calcium orthophosphates. Acta Biomaterialia. 2010. Vol. 6. pp. 715–734.
6. Uskoković V., Uskoković D. Nanosized Hydroxyapatite and Other Calcium Phosphates: Chemistry of Formation and Their Application as Drug and Gene Delivery Agents. Journal of Biomedical Materials Research B: Applied Biomaterials. 2011. Vol. 96(1). pp. 152–191. DOI: 10.1002/jbm.b.31746.
7. Dekhtyar Yu., Khlusov I., Polyaka N., Sammons R., Tyulkin F. Influence of Bioimplant Surface Electrical potential on osteoblast Behaviour and Bone Tissue Formation. IFMBE Proceeding. 2010. Vol. 29. pp. 800–803.
8. Papaspyridakos P., Mokti M., Chen C. J., Benic G. I., Gallucci G. O., Chronopoulos V. Implant and Prosthodontic Survival Rates with Implant Fixed Complete Dental Prostheses in the Edentulous Mandible after at Least 5 Years: A Systematic Review. Clinical Implant Dentistry and Related Research. 2014. Vol. 16. pp. 705-717. DOI: 10.1111/cid.12036.
9. Lopez-Noriega A., Quilan E., Celikkin N., O'Brien F. J. Incorporation of polymeric microparticles into collagen-hydroxyapatite scaffolds for the delivery of a pro-osteogenic peptide for bone tissue engineering. APL Materials 3. 2015. Vol. 3. Issue 1. Article number 014910. DOI: 10.1063/1.4902833.
10. Junqueira L. C., Carneiro J. Basic Histology: Text & Atlas. McGraw-Hill/Appleton & Lange, 2002. 10 edition. 515 p.
11. Barinov S. M., Komlev V. S. Calcium Phosphate based Bioceramics. – Moscow: Nauka, 2005 (In Russian). 204 p.
12. Nakamura Satoshi, Takeda Hiroaki, Yamashita Kimihiro. Proton transport polarization and depolarization of hydroxyapatite ceramics. Journal of Applied Physics. 2001. Vol. 89. No. 10. pp. 5386–5392.
13. Bystrov V. S., Paramonova E., Dekhtyar Y., Katashev A., Karlov A., Polyaka N., Bystrova A. V., Patmalnieks A., Kholkin A. L. Computational and experimental studies of size and shape related physical properties of hydroxyapatite nanoparticles. Journal of Physics: Condensed Matter. 2011. Vol. 23. N6. Article number 065302. DOI: 10.1088/0953-8984/23/6/065302.
14. Bystrov V. S., Bystrova N. K., Paramonova E. V., Dekhtyar Yu. D. Interaction of charged hydroxyapatite and living cells. I. Hydroxyapatite polarization properties. Mathematical biology and Bioinformatics. 2009. Vol. 4(2). pp. 7–11. URL: mathbio.org/downloads_en/Bystrov_en2009(4_7).pdf.
15. Tofail S. A. M., Haverty D., Stanton K. T., Mcmonagle J. B. Structural Order and Dielectric Behaviour of Hydroxyapatite. Ferroelectrics. 2011. Vol. 319. Issue 1. pp. 117–123.

16. Jiang W., Pan H., Cai Y., Tao J., Liu P., Xu X., Tang R. Atomic Force Microscopy Reveals Hydroxyapatite-Citrate Interfacial Structure at the Atomic Level. Langmuir. 2008. Vol. 24. pp. 12446–12451.
17. Santos C., Gomes P. S., Duarte J. A., Franke R. P., Almeida M. M., Costa M. E. V., Fernandes M. H. Relevance of the sterilization-induced effects on the properties of different hydroxyapatite nanoparticles and assessment of the osteoblastic cell response. Journal of The Royal Society Interface. 2012. Vol. 9. pp. 3397–3410. DOI: 10.1098/rsif.2012.0487.
18. PERCERAMICS: Multifunctional percolated nanostructured ceramics fabricated from hydroxyapatite, NMP3-CT-2003-504937 FP6 project, RTU, 2007, http://cordis.europa.eu/publication/rcn/12743_en.html [Reviewed 2018-04-04], Permalink: http://cordis.europa.eu/ result/rcn/51676_en.html.
19. Hertz H. Uber einen Einfluss des ultravioletten Lichtes auf die electrische Entladung. Annalen der Physik und Chemie (In German). 1887. Vol. 31. pp. 983–1000.
20. Aronov D., Chaikina M., Haddad J., Rosenman G. et al. Electronic states spectroscopy of Hydroxyapatite ceramics. Journal of Materials Science: Materials in Medicine. 2007. Vol. 18. pp. 865–870.
21. Dekhtyar Yu., Bystrov V., Khlusov I., et al. Hydroxyapatite Surface Nanoscaled characterization and Electrical Potential Functionalization to Engineer Osteoblasts Attachment and Generate Bone Tissue. Society for Biomaterials Annual Meeting. 2011. Abstract # 519.
22. Shi Z., Huang X., Cai Y., Tang R., Yang D. Size effect of hydroxyapatite nanoparticles on proliferation and apoptosis of osteoblast-like cells. Acta biomaterialia. 2008. Vol. 5(1). pp. 338–45.
23. Gullberg B., Johnell O., Kanis J. A. World-wide projections for hip fracture. Osteoporosis Int. 1997. Vol. 7(5). pp. 407–13.
24. Bystrov V. S., Paramonova E. V., Dekhtyar Yu. D., Bystrova A. V., Pullar R. C., Kopyl S., Tobaldi D. M., Piccirillo C., Avakyan L. A., Coutinho J. Surface modified hydroxyapatites with various functionalized nanostructures: Computational Studies of the Vacancies in HAP. Ferroelectrics. 2017. Vol. 509. pp. 105–112. DOI: 10.1080/00150193.2017.1294436.
25. Bystrov V. S., Piccirillo C., Tobaldi D. M., Castro P. M. L., Coutinho J., Kopyl S., Pullar R. C. Oxygen vacancies, the optical band gap (Eg) and photocatalysis of hydroxyapatite: comparing modelling with measured data. Applied Catalysis B: Environmental. 2016. Vol. 196. pp. 100–107. DOI: 10.1016/j.apcatb.2016.05.014.
26. Bystrov V., Bystrova A., Dekhtyar Y. HAP nanoparticle and substrate surface electrical potential towards bone cells adhesion: Recent results review. Advances in Colloid and Interface Science. 2017. Vol. 249. pp. 213–219. DOI: 10.1016/j.cis.2017.05.002.
27. Pankratov V., Popov A. I., Kotlov A., Feldman C. Luminescence of nano- and macrosized $LaPO_4$:Ce, Tb excited by synchrotron radiation. Optical Materials. 2011. Vol. 33. pp. 1102–1105.
28. Bystrov V. S., Coutinho J., Bystrova A. V., Dekhtyar Y. D., Pullar R. C., Poronin A., Palcevskis E., Dindune A., Alkan B., Durucan C., Paramonova E. V. Computational study of the hydroxyapatite structures, properties and defects. Journal of Physics D: Applied Physics. 2015. Vol. 48. p.195302(20 pp.).
29. Pohl H. A. The motion and precipitation of suspensoids in divergent electric fields. Journal of Applied Physics. 1951. Vol. 22. pp. 155–181.

30. Derjaguin B., Landau L. Theory of the stability of strongly charged lyophobic sols and of the adhesion of strongly charged particles in solutions of electrolytes. Acta Physico Chemica URSS. 1941. Vol. 14. pp. 633–662.
31. Bystrova A. V., Dekhtyar Yu. D., Popov A. I., Coutinho J., Bystrov V. S. Modified Hydroxyapatite Structure and Properties: Modelling and Synchrotron Data Analysis of Modified Hydroxyapatite Structure. Ferroelectrics. 2015. Vol. 475(1). pp. 135–147. DOI: 10.1080/00150193.2015.995580.
32. AIMPRO Home Page. http://aimpro.ncl.ac.uk/(accessed in May 12, 2014 and now in 2018).
33. Bystrov V. S., Paramonova E. V., Costa M. E. V., Santos C., Almeida M., Kopyl S., Dekhtyar Yu., Bystrova A. V., Maevsky E. I., Pullar R. C. and Kholkin A. L. Computational Study of the Properties and Surface Interactions of Hydroxyapatite. Ferroelectrics. 2013. Vol. 449(1). pp. 94–101. DOI: 10.1080/00150193.2013.822774.
34. Bystrov V., Paramonova E., Bystrova N., Sapronova A., Filippov S. Computational molecular nanostructures and mechanical/adhesion properties of Hydroxyapatite, Micro- and Nanostructures of Biological Systems. Aachen: Shaker Verlag, 2005. pp. 77–93.
35. Bystrov V., Bystrova N., Paramonova E., Sapronova A., Filippov S. Modeling and computation of Hydroxyapatite nanostructures and properties. Advanced materials forum III. Material Science Forum. 2006. Vol. 514–516. pp. 1434–1437. DOI: 10.4028/www.scientific.net/MSF.514-516.1434.
36. Ueshima M., Nakamura S., Yamashita K. Huge, millicoulomb charge storage in ceramic hydroxyapatite by bimodal electric polarization. Advanced Materials. 2002. Vol. 14. Issue 8. pp. 591–595.
37. Bystrov V. S., Sapronova A. V., Tazieva T. R., Green M. E. Nonlinear Dynamics of Proton Transport in Systems with hydrogen bonds. Physics of Vibrations. 2001. Vol. 9. N3. pp. 168–172.
38. Silin A. R., Trukhin A. I. Point defects and elementary excitations in crystalline and glassy SiO_2. Riga: Zinatne, 1985 (in Russian). 244 p.
39. HyperChem (2002) Tools for Molecular Modelling (release 7, 8) Professional edition. Gainesville: Hypercube, Inc. http://www.hyper.com/?tabid=360.
40. Kobayashi T., Nakamura S., Yamashita K. Enhanced osteobonding by negative surface charges of electrically polarized hydroxyapatite. Journal of Biomedical Materials Research. 2001. Vol. 57. Issue 4. pp. 477–484.
41. Bystrov V. S., Paramonova E. V., Bystrova N. K., Sapronova A. V. Hydroxyapatite polarization properties. Scientific Proceedings of Riga Technical University: Material Sciences and Applied Chemistry. 2008. Vol. 17(1). pp. 30–37.
42. Dekhtyar Yu., Bystrov V., Bystrova A., Dindune A., Katashev A., Khlusov I., Palcevskis E., Paramonova E., Polyaka N.N., Romanova M., Sammons R., Veljović D. Engineering of the Hydroxyapatite Cell Adhesion Capacity. IFMBE Proceedings. 2013. Vol. 38. pp. 182–185.
43. Dehtjars J., Līvdane A., Poļaka N., Timofeeva A. Patent: Bioprotēžu dielektriskā slāņa apstrādes paņēmiens (LR patents LV13522, 2006).
44. Zundel G. Hydrogen bonds with large proton polarizability and proton transfer processes in electrochemistry and biology. Advances in Chemical Physics. 2000. Vol. 111.
45. Slepko A., Demkov A. A. First-principles study of the biomineral hydroxyapatite. Physical Review B. 2011. Vol. 84. Article number 134108.

46. Hughes J. M., Cameron M., Crowley K. D. Structural variations in natural F, OH, and Cl apatites. American Mineralogist. 1989. Vol. 74. pp. 870–876. http://rruff.geo.arizona.edu/AMS/minerals/Hydroxylapatite.
47. Elliot J. C. Structure and Chemistry of the Apatites and Other Calcium Phosphates. Amsterdam: Elsevier, 1994. 404 p.
48. Kay M. I., Young R. A., Posner A. S. Crystal Structure of Hydroxyapatite. Nature. 1964. Vol. 204. pp. 1050–1052. DOI: 10.1038/2041050a0.
49. Bystrov V., Bystrova N., Dekhtyar Yu., et al. Size depended electrical properties of Hydroxyapatite nanoparticles. IFMBE Proceedings. 2009. Vol. 25/ VIII. pp. 230–232.